ARL-TR-8683 ● Apr 2019

DEVCOM ARMY RESEARCH LABORATORY

Electrical Arc Driven Hypersonic Projectiles

by Peter Bartkowski, Paul Berning, Casey Uhlig, and Matthew J Coppinger

NOTICES

Disclaimers

The findings in this report are not to be construed as an official Department of the Army position unless so designated by other authorized documents.

Citation of manufacturer's or trade names does not constitute an official endorsement or approval of the use thereof.

Destroy this report when no longer needed. Do not return to the originator.

ARL-TR-8683 ● APR 2019

Electrical Arc Driven Hypersonic Projectiles

by Peter Bartkowski, Paul Berning, Casey Uhlig, and Matthew J Coppinger
Weapons and Materials Research Directorate, CCDC Army Research Laboratory

REPORT DOCUMENTATION PAGE

Form Approved
OMB No. 0704-0188

1. REPORT DATE *(DD-MM-YYYY)*	2. REPORT TYPE	3. DATES COVERED (From - To)
April 2019	Technical Report	1 October 2015–31 September 2018

4. TITLE AND SUBTITLE
Electrical Arc Driven Hypersonic Projectiles

5a. CONTRACT NUMBER

5b. GRANT NUMBER

5c. PROGRAM ELEMENT NUMBER

6. AUTHOR(S)
Peter Bartkowski, Paul Berning, Casey Uhlig, and Matthew J Coppinger

5d. PROJECT NUMBER

5e. TASK NUMBER

5f. WORK UNIT NUMBER

7. PERFORMING ORGANIZATION NAME(S) AND ADDRESS(ES)
US Army Combat Capabilities Development Command
Army Research Laboratory
ATTN: FCDD-RLW-PE
Aberdeen Proving Ground, MD 21005

8. PERFORMING ORGANIZATION REPORT NUMBER
ARL-TR-8683

9. SPONSORING/MONITORING AGENCY NAME(S) AND ADDRESS(ES)

10. SPONSOR/MONITOR'S ACRONYM(S)

11. SPONSOR/MONITOR'S REPORT NUMBER(S)

12. DISTRIBUTION/AVAILABILITY STATEMENT
Approved for public release; distribution is unlimited.

13. SUPPLEMENTARY NOTES

14. ABSTRACT
The US Army Combat Capabilities Development Command's Army Research Laboratory has developed a research gun capable of firing small projectiles of less than 1 g at velocities over 3000 m/s. This gun is powered via a high-voltage electrical discharge rather than conventional propellants. A 20-kV, 188-µF capacitor bank is used to power the gun. Vaporization of a copper electrode creates a pressure in the breech that propels the projectile forward down the barrel. Several different design variables were explored to determine their effect on projectile velocity. The variable that had the largest effect on projectile velocity was the strength of the steel barrel. Computer simulations of the gun performance matched well with the experimental results.

15. SUBJECT TERMS
hypersonic projectiles, arc, high voltage, capacitor, gun, vaporization

16. SECURITY CLASSIFICATION OF:			17. LIMITATION OF ABSTRACT	18. NUMBER OF PAGES	19a. NAME OF RESPONSIBLE PERSON
a. REPORT	b. ABSTRACT	c. THIS PAGE			Peter Bartkowski
Unclassified	Unclassified	Unclassified	UU	54	19b. TELEPHONE NUMBER (Include area code) 410-278-0210

Contents

List of Figures

List of Tables

Acknowledgments

This work was supported in part by a grant of computer time from the Department of Defense High Performance Computing Modernization Program at the US Army Combat Capabilities Development Command's Army Research Laboratory's Department of Defense Supercomputing Resource Center and the Terminal Ballistics Frontier project.

1. Introduction

The US Army Combat Capabilities Development Command (CCDC) Army Research Laboratory (ARL) has developed a research gun capable of firing small cylindrical projectiles over 3 km/s using only electricity as its energy source. It is not a magnetic launch system, but rather utilizes an electrical arc to produce a rapidly expanding gas that is used as the propellant. The main advantage of this system over conventional solid-propellant-driven projectiles is the ability to flip a switch to convert the system into a safe state that does not have any hazards. However, this type of system also comes with significant integration burdens such as the large volume and weight associated with a conventional high-voltage capacitor necessary to store the electrical energy required to power the gun.

2. Prior Work

A series of experiments were performed as proof of concept that an electrically powered research gun could propel small cylindrical projectiles to hypersonic velocities. The system consisted of a high-voltage capacitor that stored the electrical energy, and a mechanically operated high-voltage switch connected to the anode of the gun. The gun barrel acted as the cathode.

The capacitor, shown in Fig. 1, was a model 32511 Energy Storage Capacitor manufactured by Maxwell. It had a nominal capacitance of 175 μF and was charged to a maximum voltage of 20 kV. This yielded a maximum stored energy of 35 kJ. The capacitor was connected to the test stand with 100-mm-wide × 0.5-mm-thick copper striplines. The test stand incorporated a manual switch and mounting provisions for the barrel. Figure 2 shows the switch, which is a simple stripline conductor with a string attached. To discharge the capacitor and fire the gun, the string is pulled, moving the stripline to make contact with a copper contact bar at the top of the frame, which is connected to the electrode placed in the end of the barrel. Another stripline connects the barrel to the ground side of the capacitor, completing the circuit. Several different projectiles were investigated, with the most common being a simple right circular cylinder of aluminum with a length-to-diameter ratio of 1.0. A few experiments were also conducted using spherical projectiles of the same diameter.

Fig. 1 High-voltage capacitor

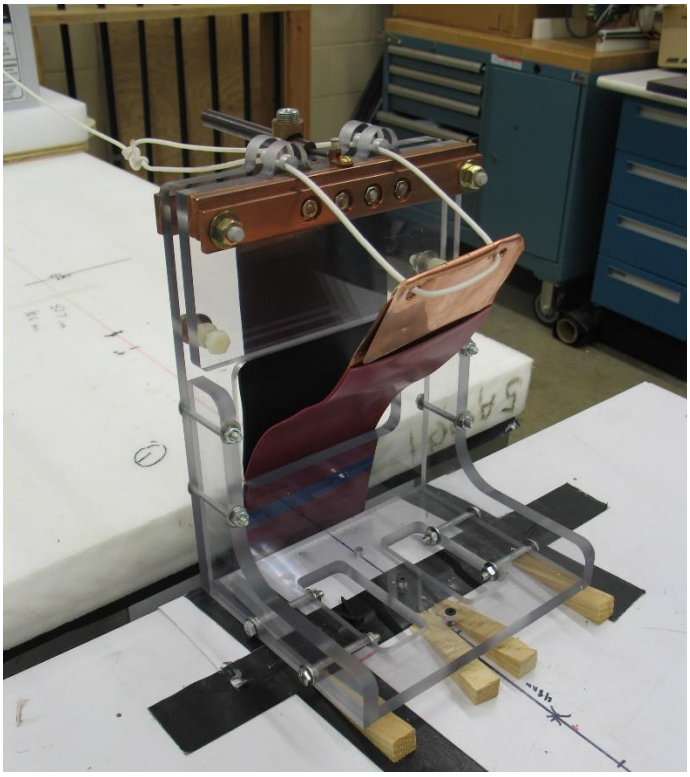

Fig. 2 Close-up of test stand

The barrel was made from 15.9-mm-diameter 17-4 PH steel, drilled along the centerline to create a 100-mm-long barrel. A 3.81-mm-diameter hole was drilled from the opposite end for the electrode. The electrode was a piece of copper rod

with a tapered point ground on one end. A sleeve of PVC insulation was placed on the rod to insulate it from the hole in the barrel. Epoxy was used to fill the void between the tapered tip and the insulating sleeve. The system was assembled by inserting the tapered point of the electrode into the breech end of the gun barrel and then inserting the projectile into the muzzle end of the barrel and sliding it down the barrel with a push rod until it contacted the electrode tip (Fig. 3).

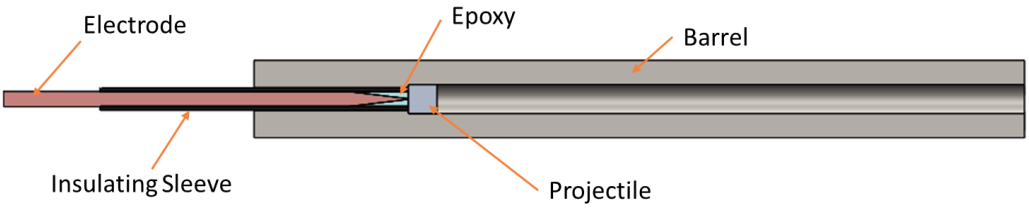

Fig. 3 Cross section of barrel assembly

A series of experiments were performed to understand what design parameter affected projectile velocity the most. These yielded projectile velocities between 1790 to 2630 m/s for a 4.76-mm-diameter aluminum projectile with a length/diameter ratio of 1.0 (more detail can be found in Appendix A). Velocity proved to be sensitive to the taper on the electrode with the optimum length being approximately 4× the diameter. Spherical projectiles performed worse than cylindrical ones. This is attributed to the cylindrical projectiles making a better seal with the barrel, preventing blow-by of the propelling gases.

3. System Design

In an effort to improve system performance and repeatability, the system was redesigned. The capacitor bank was upgraded, the electrode and insulator were redesigned, and the outer diameter of the barrel was increased. These changes resulted in experimental velocities that were very reproducible and were used as a testbed for characterizing the system performance and evaluating ideas for improvement.

The system has the same basic operation as the prior work. The test stand was redesigned to increase strength and operational ease (Fig. 4). The new design also incorporated a hinged lever to operate the switch and had replaceable arc contacts. As with the previous design, once the high-voltage capacitor is charged, the string is pulled to mechanically close the switch and fire the gun. Copper clamps were machined to mechanically clamp and conduct electricity to the barrel and electrode.

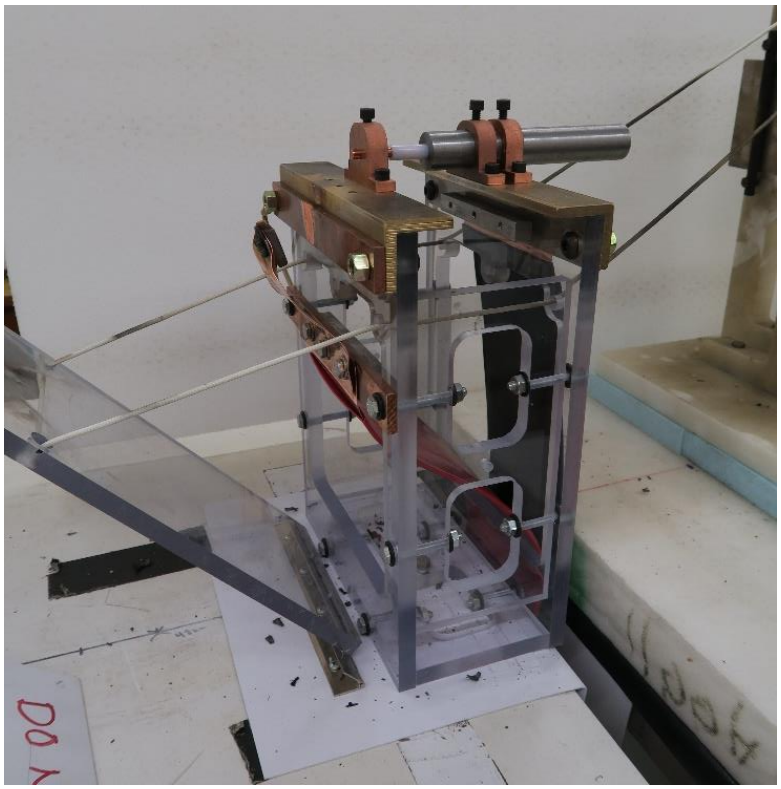

Fig. 4 New test stand

The previous single capacitor was replaced with a capacitor bank consisting of three ICAR Bioenergy D-65B 62.5–2000 capacitors in parallel (Fig. 5). These capacitors have a nominal capacitance of 62.5 µF each and can be charged up to 20 kV potential. This yields a maximum stored energy of 37.5 kJ for the capacitor bank. The advantage of using three parallel capacitors, as opposed to the single capacitor, is the increased current handling capacity. The ICAR Bioenergy capacitors were designed for nominal discharges up to 130-kA peak current each, yielding a total peak current rating of 390 kA. The Maxwell capacitor is only rated to 50-kA peak current, which resulted in the failure of several of these capacitors after a number of discharges at 300–400 kA.

Fig. 5 New ICAR Bioenergy capacitor bank

The barrel, electrode, and insulating sleeve underwent a significant redesign (see Fig. 6). The barrel is larger in diameter at 25.4 mm and made from 4340 alloy steel. The barrel has the same nominal inner diameter and length as before, but is reamed to improve the surface finish and projectile to barrel fit. The electrode body has a larger 6.35-mm diameter with a reduced diameter machined tip. A larger diameter Polytetrafluoroethylene (PTFE) insulating sleeve is used to match the 6.35-mm-diameter electrode and 9.52-mm-diameter hole forming the breech of the barrel. As before, epoxy fills the void between the electrode tip and insulating sleeve. The projectile is the same 4.76-mm diameter, L/D = 1, 7075 aluminum cylinder as before.

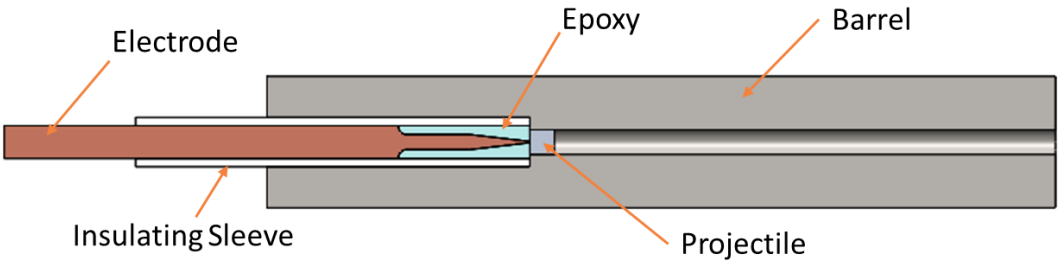

Fig. 6 New gun assembly cross section

Different electrode tip geometries were investigated in this report. Several experiments were done with a simple tip geometry of a cylinder with a point on the end. Two different nominal diameters were used with four different L/D ratios for the point, as shown in Fig. 7. The performance of electrode geometry D was used as a baseline for performance of all the other designs.

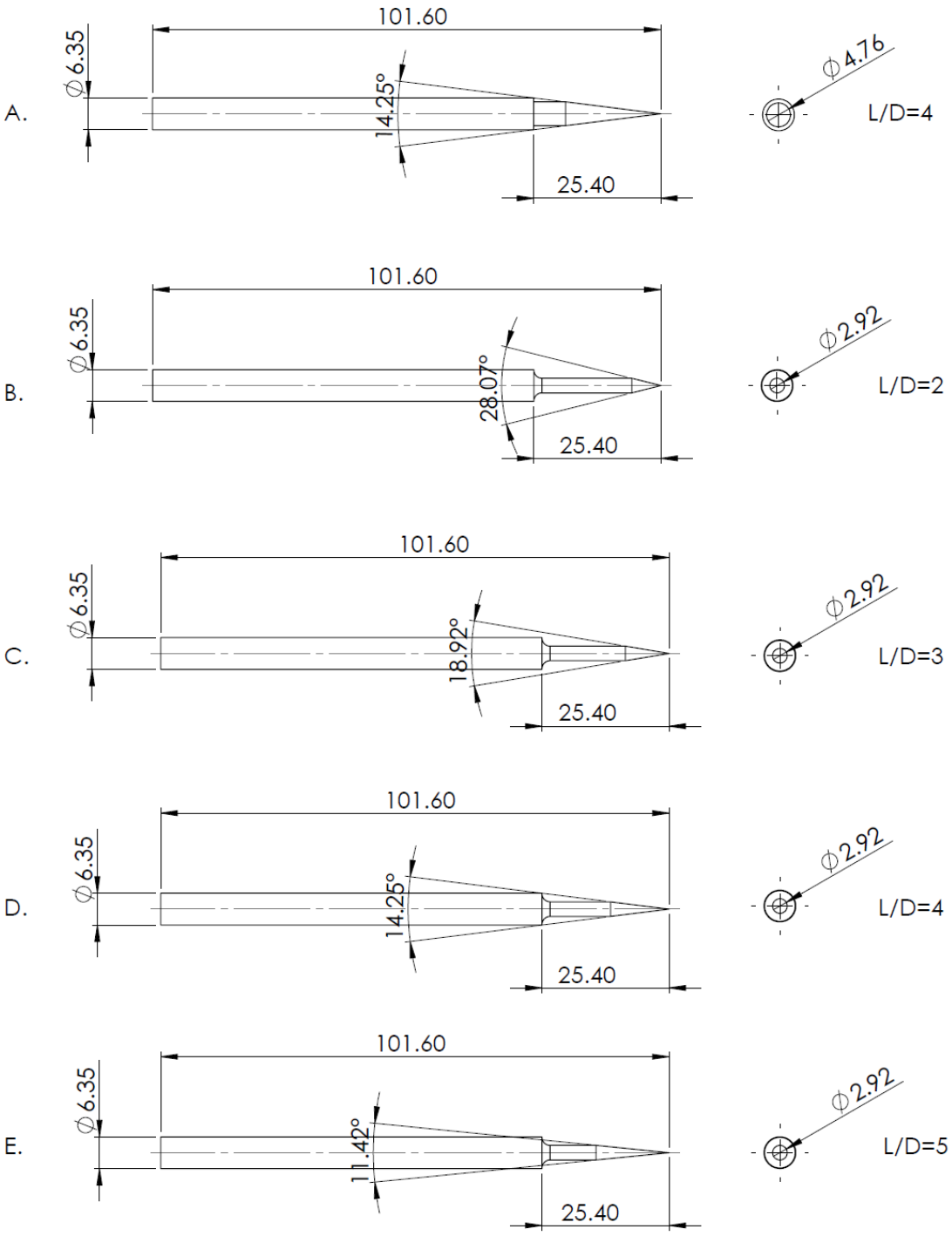

Fig. 7 Electrodes with simple point geometries

Four other more complex tip geometries were also investigated, shown in Fig. 8. Three of these were made by inserting copper tubing into a hole drilled in the end of the 6.35-mm-diameter rod. All the copper tubes had a wall thickness of 0.4 mm. Electrode F had a set of stepped concentric tubes that decreased in diameter to the tip. The tips of electrodes G and H were soldered into place, while electrode F was epoxied into place. Electrode I was similar to the simple points in Fig. 7, but had a more complex geometry consisting of three different tapers.

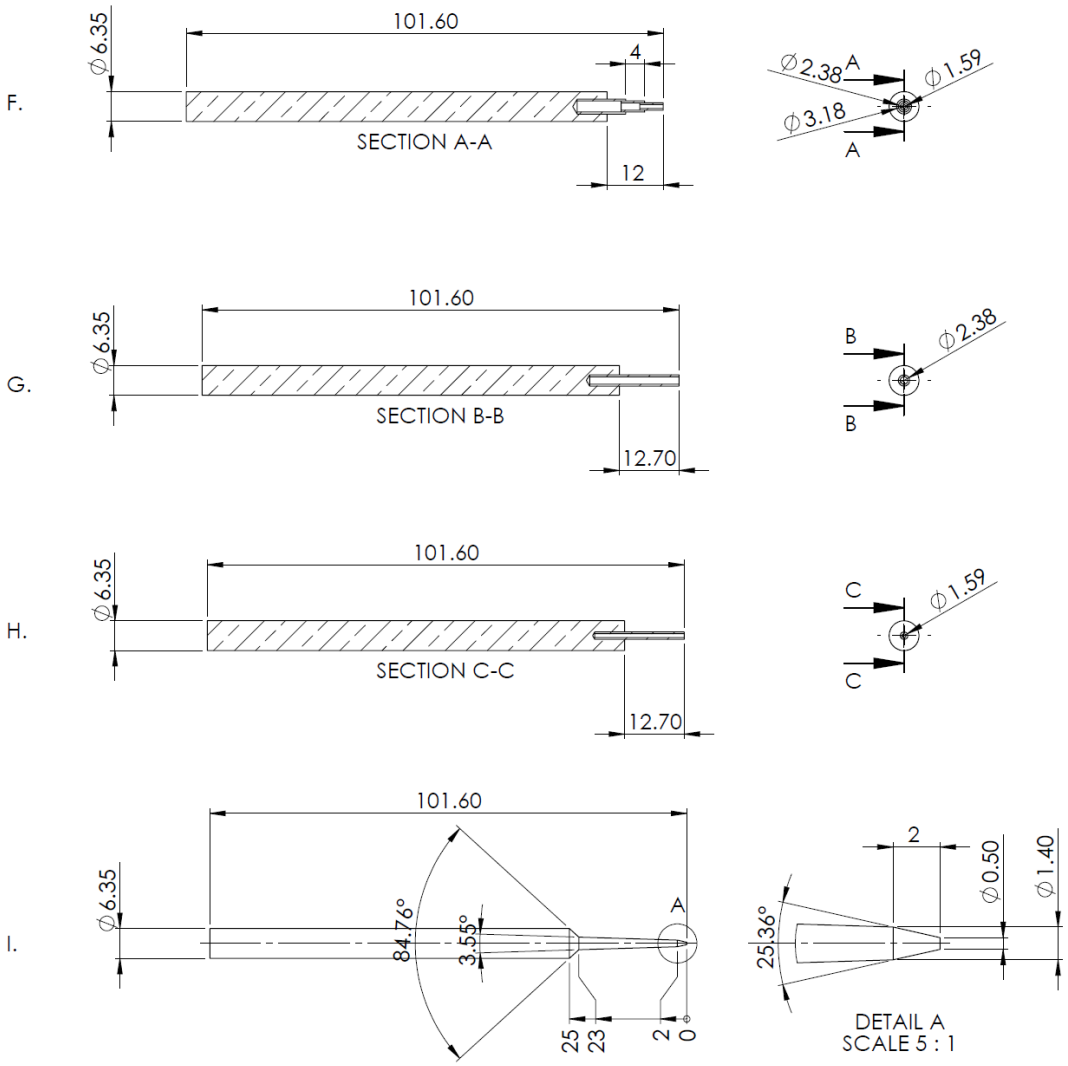

Fig. 8 Electrode with complex tip geometries

4. Instrumentation

There were three quantities measured during the experiments: the electrical current and voltage at the test stand, and the projectile velocity. Electrical current was measured using a Rogowski probe manufactured and calibrated at ARL. The Rogowski cable was wrapped around one of the transmission lines from the capacitor bank to the test stand. It sensed the derivative (di/dt) of the current, which was attenuated and recorded on an Agilent Technologies DSO6104A digital oscilloscope. The di/dt waveform was then numerically integrated to produce a current versus time trace.

Voltage was measured using two Northstar PVM-2 40-kV high-voltage probes. A probe was attached to each conductor (positive and negative) of the test stand. The two signals were then subtracted from each other to determine the voltage across the test stand during the capacitor discharge. Using this voltage and the current, the energy delivered to the test stand was calculated.

Projectile velocity was measured using several different techniques during this test series. The first technique, shown in Fig. 9, used three make screens separated by 20-cm line of sight to detect the projectile time of arrival. From this, two average velocity measurements were made starting at 25 cm from the barrel muzzle. The three make screens were 0.025-mm aluminum foil along with photodiode light detectors. The impact of the aluminum projectile with the make screen produces a flash of light detected by the photodiodes. The photodiode signals were recorded on another Agilent Technologies DSO6104A digital oscilloscope. The timing between the flashes of light along with the distance measured between the screens allows calculation of the average projectile velocity between the screens.

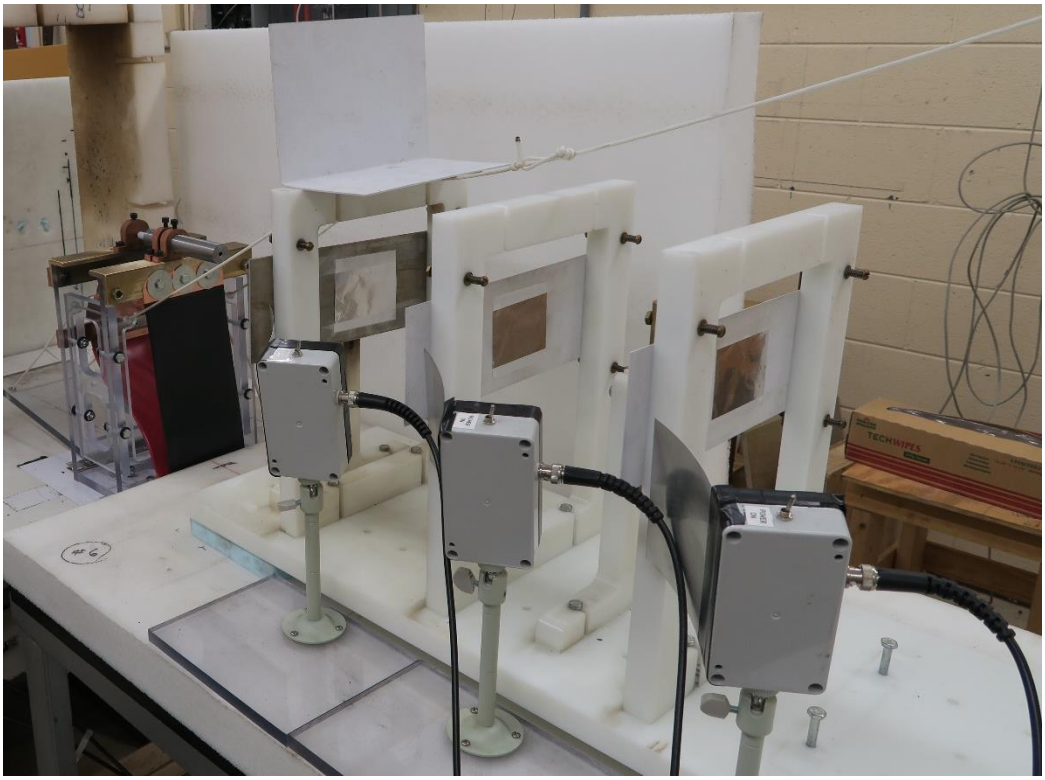

Fig. 9 Make screens and photodiode detectors for measuring projectile velocity

The second technique used high-speed (HS) video to film the projectile flight. From this video, position versus time was analyzed to determine projectile velocity. This produced good results; however, there were some experiments where the projectile was obscured by gasses emerging from the gun tube. There is likely some blow-by that escapes around the fit between the projectile and barrel and travels in front of the projectile. The projectile typically outruns these gases after traveling 10–20 cm downrange.

The third technique[1] used magnetic pickup sensors to detect the passage of the projectile in time. Signals from two sensors placed 10 cm apart were recorded on another Agilent Technologies DSO6104A digital oscilloscope. Each sensor consisted of a powerful permanent magnet ring followed by an adjacent coil wound from magnet wire. As the projectile passes through the permanent magnet shown in Fig. 10, a magnetic field is induced within the projectile. The coil senses the change in magnetic flux as the projectile passes through it. The average velocity was calculated from the time interval recorded on the oscilloscope and distance between the two sensors.

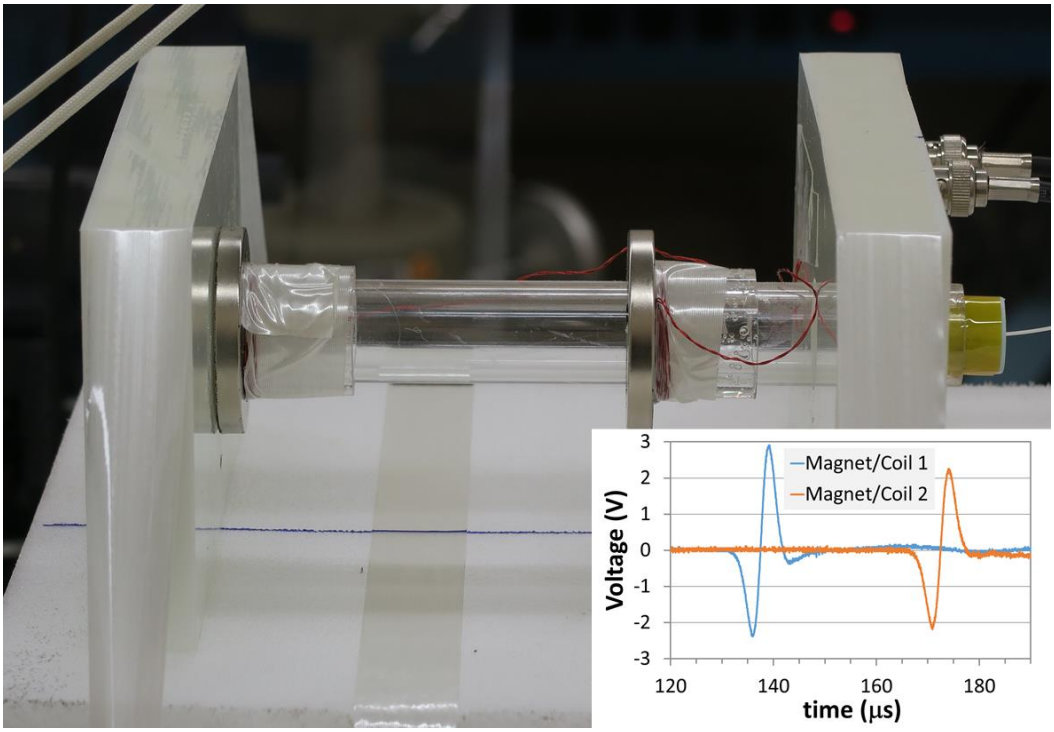

Fig. 10 Magnetic pickup sensors used to measure projectile velocity. The inset shows the induced voltage on the sensing coils as a projectile traverses the apparatus.

The fourth technique used Photon Doppler Velocimetry (PDV) to record the projectile velocity.[2] The PDV system uses a laser to track the velocity of a surface. The Doppler shift imparted to the reflected laser beam is recorded and then analyzed to give a projectile velocity with time. One significant advantage of the PDV system is that the laser is capable of looking down the barrel of the gun, thus providing a complete velocity history of the projectile during acceleration in the barrel and free flight out of the barrel. The fiber optic cable and probe can be seen inserted in the right end of the Lexan tube in Fig. 10.

5. Experiments

In all, 18 experiments were performed, 17 of which are reported here. Table 1 is a summary of the experimental test results. Electrode geometries are designated by letters represented in Figs. 7 and 8. The column Charge Voltage is the voltage the capacitor bank is charged to before firing the gun. Energy is the calculated initial stored energy in the capacitor bank. Fixture Energy is the final energy delivered to the fixture that the gun is mounted to, some of which is transmitted to the fixture after the projectile leaves the barrel. The difference between stored energy and fixture energy is lost during transmission to the gun. Velocity of the projectiles as measured using the four different techniques is reported in the last four columns. In

each experiment, two velocity-measuring techniques were employed. The first five experiments used the make light and HS video to measure the projectile velocity. In general, the HS video velocity is higher than the make light velocity. This is due to the HS video measurement being made closer to the muzzle than the make light screens. The velocity of the projectile does drop as it flies downrange due to aerodynamic drag. The same effect can be seen between the PDV projectile velocity and the magnetic pickup velocity. The PDV measurement yields the peak velocity of the projectile as it exits the muzzle, while the magnetic pickup sensors are located downrange and thus record a lower velocity.

Table 1 Summary of experimental results

		Elect.	Charge	Energy	Fixture	Velocity (m/s)			
Shot #	Description	Geom.	Voltage (kV)	(kJ)	E (kJ)	Make light	HS video	Mag pickup	PDV
1	2.92-mm dia L/D = 4 tip	D	10	9.5	6.98	1703	1740	NA	NA
2	2.92-mm dia L/D = 4 tip	D	15	21.4	15.2	2519	2540	NA	NA
3	2.92-mm dia L/D = 4 tip	D	20	38.0	21.8	2953	2970	NA	NA
4	Repeat of #3	D	20	38.0	23.9	2971	2940	NA	NA
5	2.38-mm dia Cu tube	G	20	38.0	16.8	1980	1940	NA	NA
6	Repeat of #3 with PDV	D	20	38.0	17.9	NA	NA	2920	2978
7	1.59-mm dia Cu tube	F	20	38.0	12.0	NA	NA	2530	2555
8	2.92-mm dia L/D = 2 tip	B	20	38.0	18.3	NA	NA	2500	2590
9	Hard steel barrel	D	20	38.0	26.1	NA	NA	3305	3410
10	Complex electrode tip	I	20	38.0	25.0	NA	NA	2870	2950
11	2.77-mm dia L/D = 3 tip	C	20	38.0	23.7	NA	NA	2985	3070
12	2.87-mm dia L/D = 5 tip	E	20	38.0	21.5	NA	NA	2865	2950
13	Ti pellet	D	20	38.0	25.4	NA	NA	2180	2223
14	4.76-mm dia L/D = 4 tip	A	20	38.0	24.2	NA	NA	3040	3132
15	Hard barrel, stepped tube tip	F	20	38.0	16.6	NA	NA	2640	2698
16	Data not reported								
17	Mica insulator	D	20	38.0	22.9	NA	NA	2577	2674
18	Bakelite insulator	D	20	38.0	14.6	NA	NA	2363	2449

Notes: Cu = copper; Ti = titanium.

Experiments 1–4 were performed to shakedown the new capacitor bank. The first three experiments increased the charge voltage from 10 to 20 kV. Experiment 4 was a repeat of experiment 3 to get an idea of projectile velocity repeatability. All of these experiments used our baseline electrode design geometry D and an aluminum projectile. As expected, as the stored energy is increased, there is a corresponding increase in projectile velocity. Electrical current discharged from the capacitor bank for each experiment is shown in Fig. 11. The peak current into the gun during experiment 1 was 191 kA and experiment 2 had a peak of 283 kA. The peak current in experiment 3 and the repeat experiment 4 was 348 and 378 kA, respectively. The increase in current between experiments 3 and 4 is attributed to the repositioning of the transmission lines between the capacitor bank and the test fixture. The transmission lines will move apart from each other due to the strong repulsive magnetic field generated during the discharge. Repositioning the transmission lines closer together reduces the inductance, creating a shorter current rise time and higher peak currents. The transfer efficiency does drop as the voltage/current is increased, from 73% at 10-kV charge voltage to an average of 60% at the 20-kV charge voltage. Averaging all four of the velocities recorded in experiments 3 and 4 yields an average velocity of 2959 m/s; 14% higher than the peak velocity in the prior work.

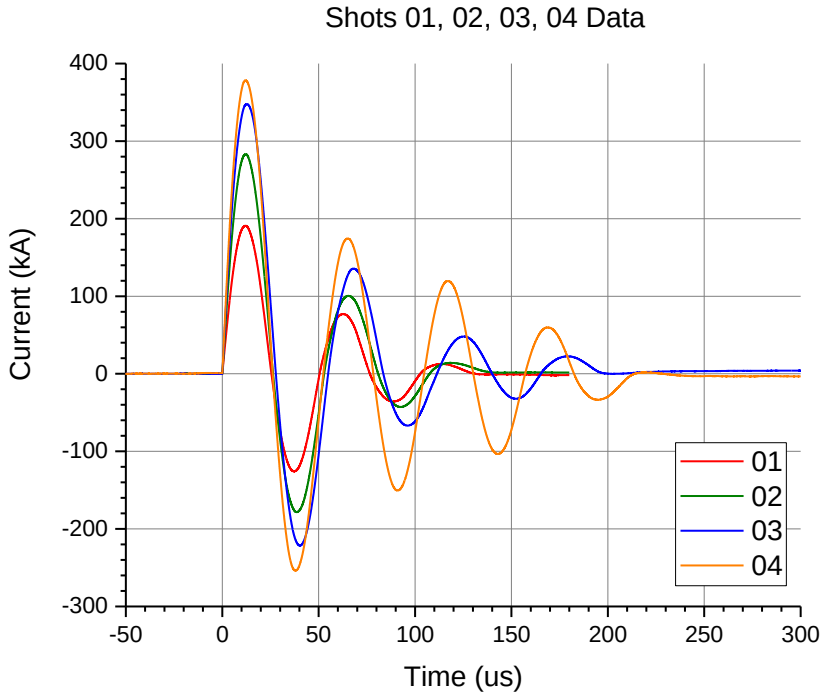

Fig. 11 Experimental capacitor current for experiments 1–4

Experiments 5 and 7 used a different electrode geometry. The tips were created by soldering copper tubes into a hole drilled in the end of the electrode rod. These two experiments resulted in lower projectile velocities than the baseline tip. Figure 12 shows the electrical current discharged from the capacitor bank and the velocity measured via the PDV system for experiments 6 and 7. Experiment 6 is a repeat of experiments 3 and 4, but with the addition of the PDV velocity measurement. It has been added to these other two experiments for comparison. As can be seen in Fig. 12, the peak current for all three experiments was nearly identical. Projectile velocity, however, was lower from the two tube-shaped tips. The PDV projectile velocities appear to peak 5–10 μs after the projectile leaves the muzzle (see Appendix B for plots that contain electrical current, projectile velocity, and position). For experiments 6 and 7, the projectile leaves the muzzle at 48 μs and 56 μs, respectively.

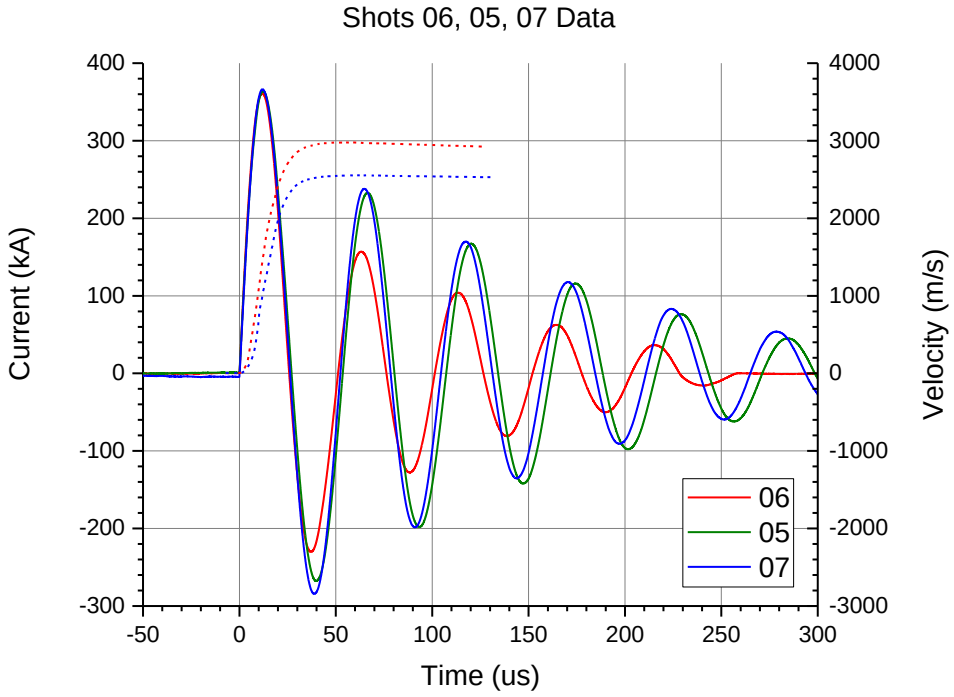

Fig. 12 Experimental capacitor current and PDV velocity for experiments 5–7

The capacitor current and PDV velocity for experiments 10 and 14 are shown in Fig. 13. Experiment 10 used a complex electrode tip geometry, which consisted of three different taper angles. Experiment 14 was a simple L/D = 4 tip geometry, but the diameter was larger at 4.76 mm. The performance of the complex tip was consistent with our standard 2.9-mm-diameter, L/D = 4 tip taper. The larger diameter of experiment 14 produced a slightly higher muzzle velocity of 3132 m/s.

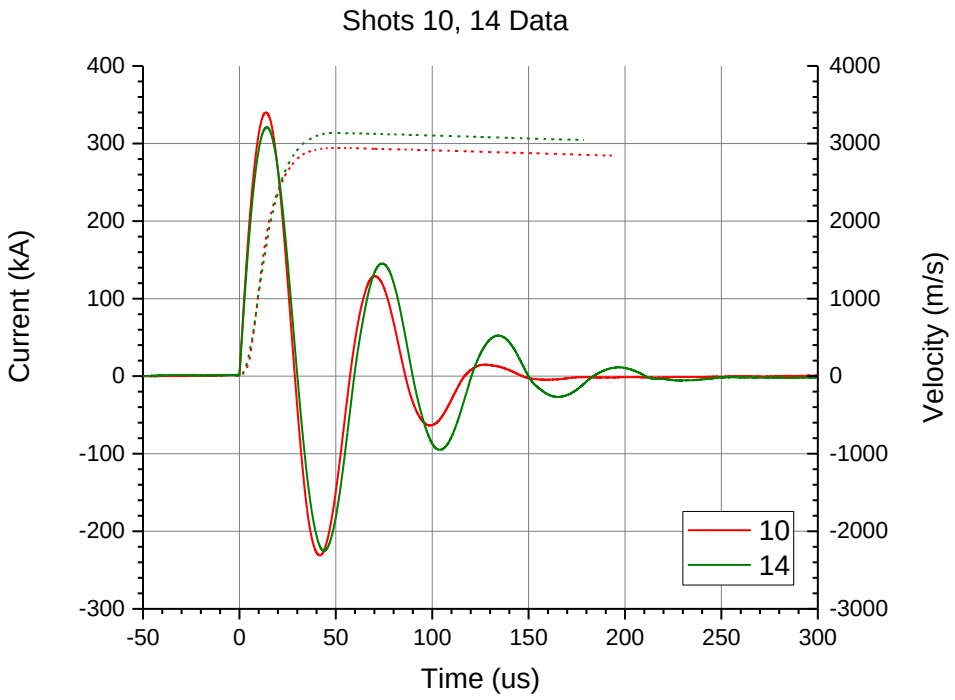

Fig. 13 Experimental capacitor current and PDV velocity for experiments 10 and 14

Experiments 8, 11, and 12 explored the effects of different tapers on the end of the electrode. Experiment 8 had an L/D ratio of 2, experiment 11 had a ratio of 3, and experiment 12 had a ratio of 5. Figure 14 shows the current recorded during each experiment along with the PDV projectile velocity. The L/D = 2 ratio had a lower muzzle velocity of only 2590 m/s, significantly lower than the standard L/D = 4 tip. The L/D = 5 ratio produced a muzzle velocity of 2950 m/s, which is comparable to the L/D = 4 ratio. Experiment 11's L/D = 3 ratio produced a slightly higher muzzle velocity of 3070 m/s.

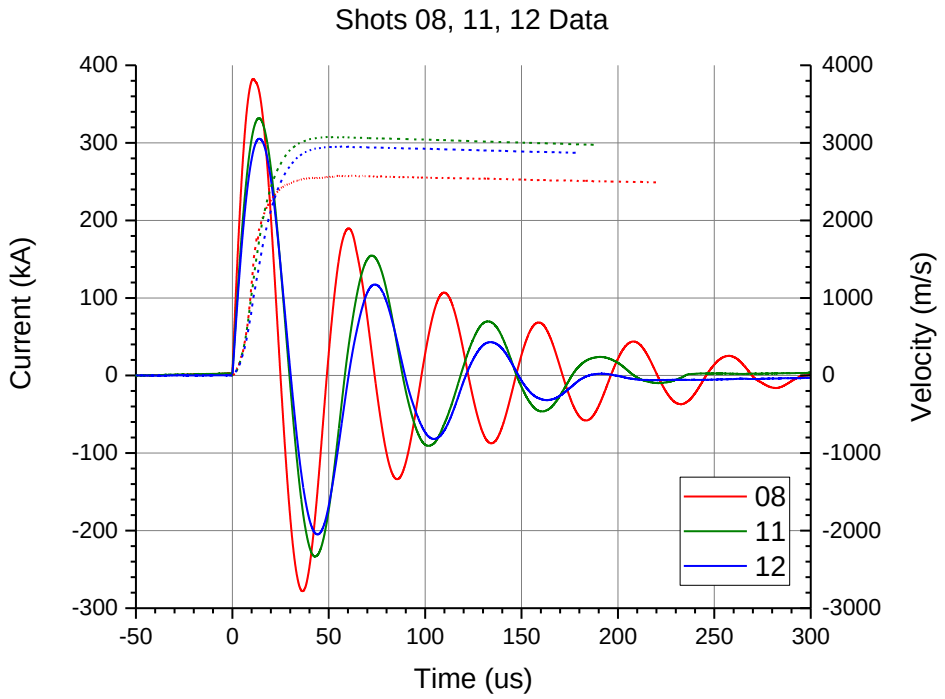

Fig. 14 Experimental capacitor current and PDV velocity for experiments 8, 11, and 12

Experiment 13 was conducted using the standard tip but used a titanium projectile instead of aluminum. With the higher mass projectile, a lower projectile muzzle velocity of 2223 m/s was observed (as can be seen in Fig. 15). Correspondingly, the time to exit the barrel was longer at 63 µs. Assuming the mass of the projectiles remains constant during the launch process, the kinetic energy of the titanium projectile at muzzle velocity is 0.936 kJ. This is comparable to the aluminum projectile muzzle kinetic energy of 1.06 kJ calculated in experiment 6.

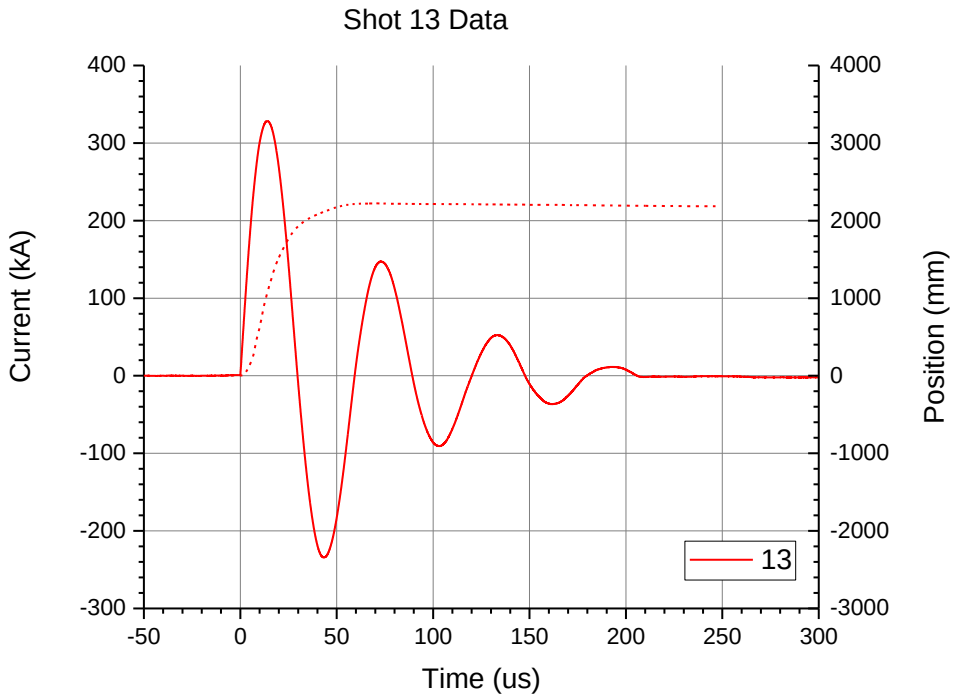

Fig. 15 Experimental capacitor current and PDV velocity for experiment 13

Experiments 17 and 18 investigated the effect of changing the PTFE insulating sleeve placed around the electrode. It was observed in the previous experiments that the PTFE sleeve was being extruded out of the back of the breech during the gun firing. Two experiments were conducted using stiffer insulating sleeves around the standard electrode, in the hope that they would help confine the breech pressure more, resulting in higher projectile velocities. Experiment 17 used a mica insulating sleeve and experiment 18 used a Bakelite insulating sleeve. As can be seen in Fig. 16, both materials had the opposite effect and resulted in lower projectile velocities. The mica insulator produced a muzzle velocity of 2674 m/s, while the Bakelite insulator resulted in a muzzle velocity of only 2449 m/s.

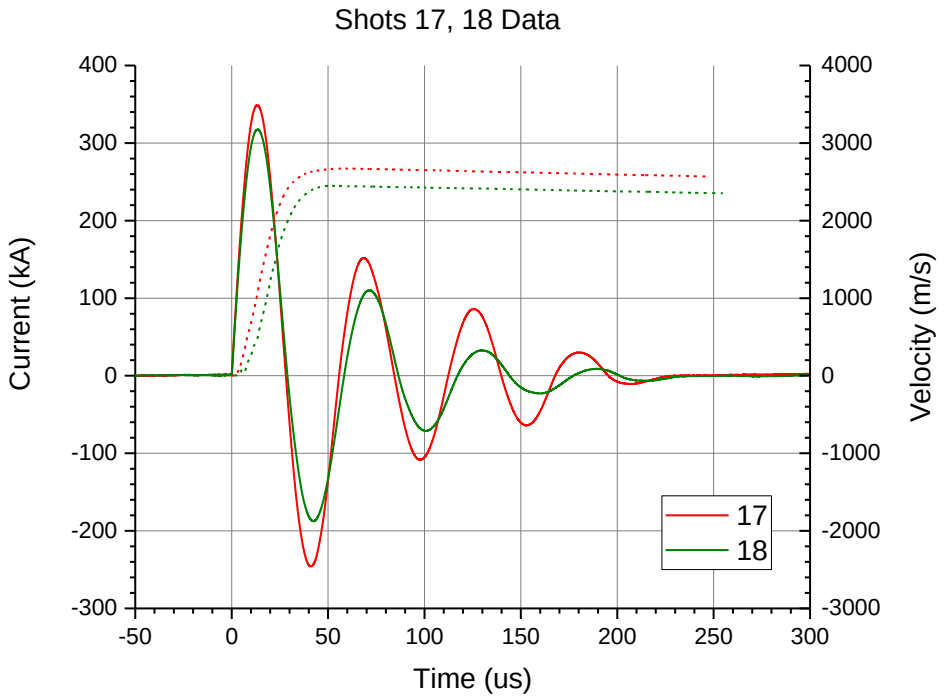

Fig. 16 Experimental capacitor current and PDV velocity for experiments 17 and 18

Experiments 9 and 15 were conducted using 4340 steel that had been hardened through heat treating. The stock 4340 steel used in all the other experiments had a Brinell hardness of 217 at the outer surface (207 at the center). After heat treating, the steel reached a Brinell hardness of 387. These hardnesses correspond to a steel strength of 731 MPa (695 MPa center) for the stock steel and 1276 MPa for the hardened steel. Experiment 15 used a tip consisting of concentric copper tubes. This combination of hardened barrel and tip design resulted in a lower projectile muzzle velocity of only 2698 m/s. Experiment 9 used the standard 2.92-mm-diameter, L/D = 4 tip. This combination of hardened steel barrel and standard tip produced a 15% increase in projectile muzzle velocity. The PDV system (see Fig. 17) measured the velocity at 3410 m/s. The barrels from experiments 3 and 9 were sectioned to observe the deformation to the breech (see Fig. 18). The top image shows the stock 4340 steel barrel and the bottom image is the hardened 4340 steel. It is obvious that the lower Brinell hardness of the stock steel had more deformation in the breech and bore entrance. The hardened steel barrel only has a small amount of deformation near the bore entrance. Minimizing breech volume expansion apparently produces higher projectile acceleration forces, resulting in a higher overall projectile velocity.

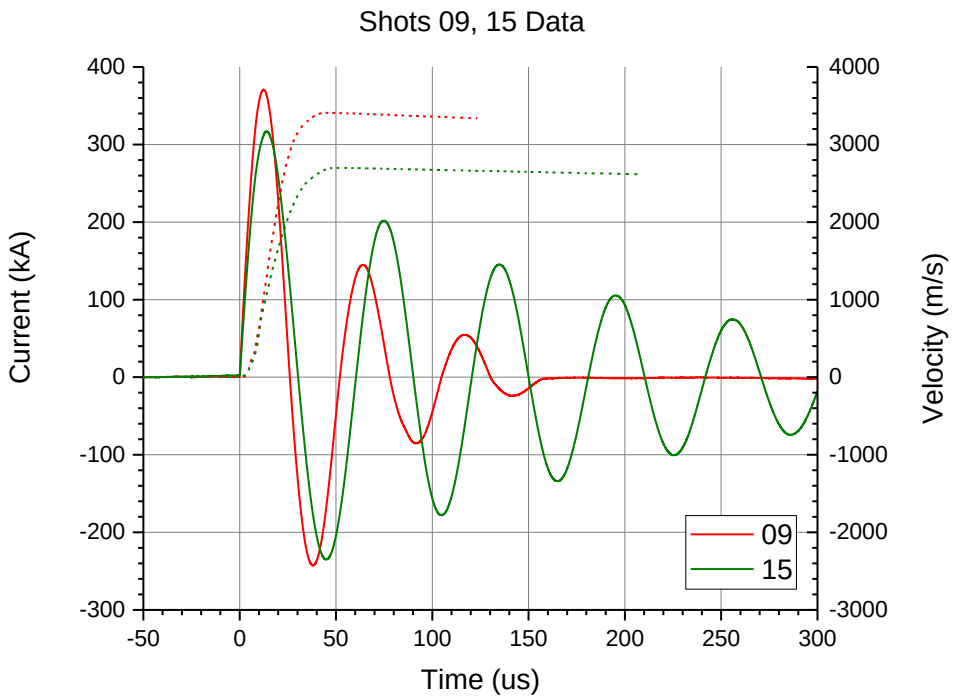

Fig. 17 Experimental capacitor current and PDV velocity for experiments 9 and 15

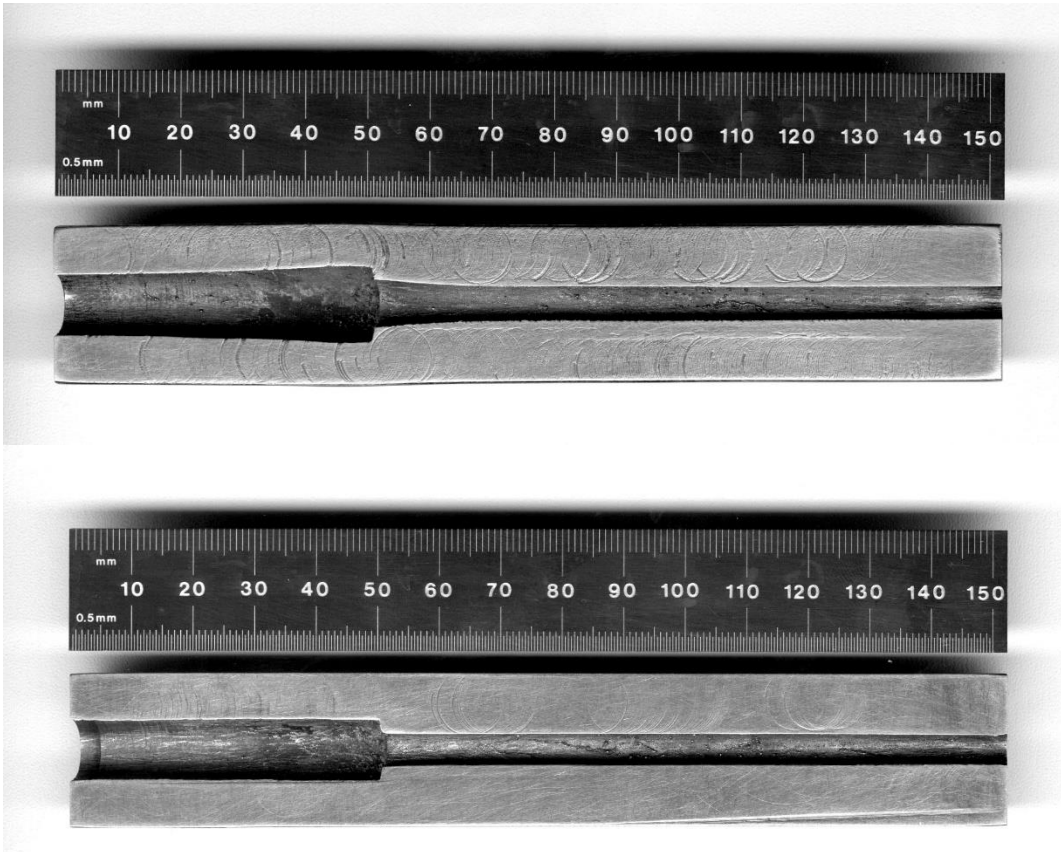

Fig. 18 Sectioned barrels from experiments 3 and 9

6. Simulations

Three-dimensional simulations of the thermal-electric device were performed using the shock physics code ALEGRA with magnetohydrodynamic capabilities developed by Sandia National Laboratories.[3] A cylindrical trisection mesh, with 1/4 symmetry and cells with edges less than 0.1 mm in the region of the electrode tip, was utilized. A material model for Lexan was used in place of the epoxy and polyethylene tube surrounding the electrode, and a simple elastic-plastic model in which the yield strength was varied was used for the steel barrel. An external circuit was applied to the mesh, which included a capacitor, resistor, and inductor with electrical feeds going to the copper electrode (hot lead) and the end of the barrel (zero potential). The capacitance, resistance, and inductance of the external circuit elements were set at 191 μF, 10.4 mΩ, and 340 nH, respectively. The capacitance was based on the measured value in the experimental apparatus. The resistance and inductance were chosen to produce current versus time curves somewhat in the middle of the experimentally measured curves, which varied appreciably from shot to shot. Figure 19 shows the experimental curves of shot 3, 4, and 11 in comparison to the current produced in the simulations for three different tip geometries, L/D = 3, L/D = 4, and L/D = 5, respectively. It is readily seen that the simulations vary only slightly with the change in electrode geometry and attain a peak current of 350 kA, which is in the approximate median range of the experimental peak currents. An LCR fit of the three experimental curves gives values of 400 nH and 13.8 mΩ, 355 nH and 11 mΩ, and 450 nH and 12.5 mΩ for shots 3, 4, and 11, respectively. While the resistance chosen for the simulation is slightly lower than the experiment, it is important to note that the experimental fit is the total resistance and the simulation circuit resistance is exclusively external to the gun. Experimental components contained within the simulation mesh also contribute to the total resistance in the simulation. While no attempt was made to identically fit the simulation current to each experiment, the simulation currents fit well within the experimental range.

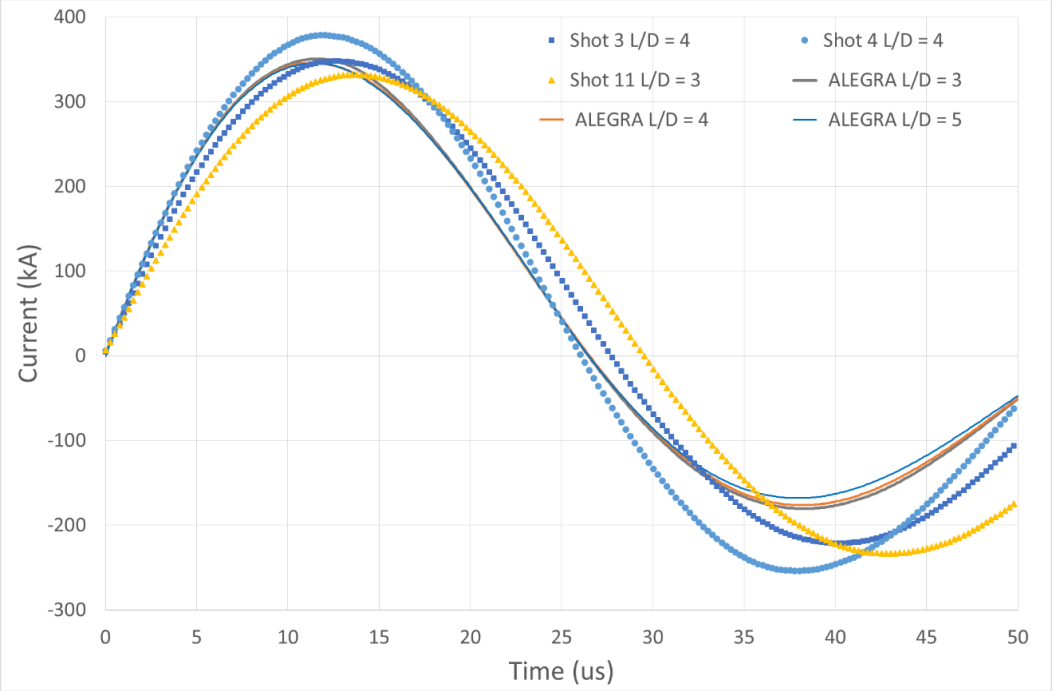

Fig. 19 Comparison of applied current observed in multiple shots to the resulting current from ALEGRA simulations

Color maps of the current density as a function of time for an L/D = 4 electrode is shown in Fig. 20, which contains a mirrored slice of the simulation to visualize the entire electrode, projectile, and barrel. The current density is shown on a log scale from 1×10^{8} to 1×10^{11} A/m^3. Copper vaporization and/or wire explosion on the microsecond timescale typically requires current densities approaching 1×10^{11} A/m^3, observed here only in the tip region of the electrode. The current is initially isolated to just the outer surfaces flowing along the copper electrode to the projectile and out along the inner surface of the barrel, but gradually soaks into the material.

Small amounts of current trail along with the projectile as it traverses the barrel, but after initial vaporization of the very end of the electrode tip and cratering the pellet, the current density in the pellet is not sufficient to cause further damage or erosion. As the copper electrode vaporizes, a plasma surrounding the tip is formed, and pressures over 5 GPa develop within the chamber. Insulating material surrounding the tip is compressed and flows outward, creating a cavity, and some of the material is eroded and mixed into the plasma. Additionally, the barrel chamber is observed to expand. The barrel yield strength was set to 695 MPa, which corresponds to the measured Brinell hardness of 207 at the center of the stock barrel material as purchased. A superposition of the barrel expansion produced in the simulations to

the barrel sectioned from shot 3 is shown in Fig. 21, where the blue outline overlaying the image represents the simulated barrel.

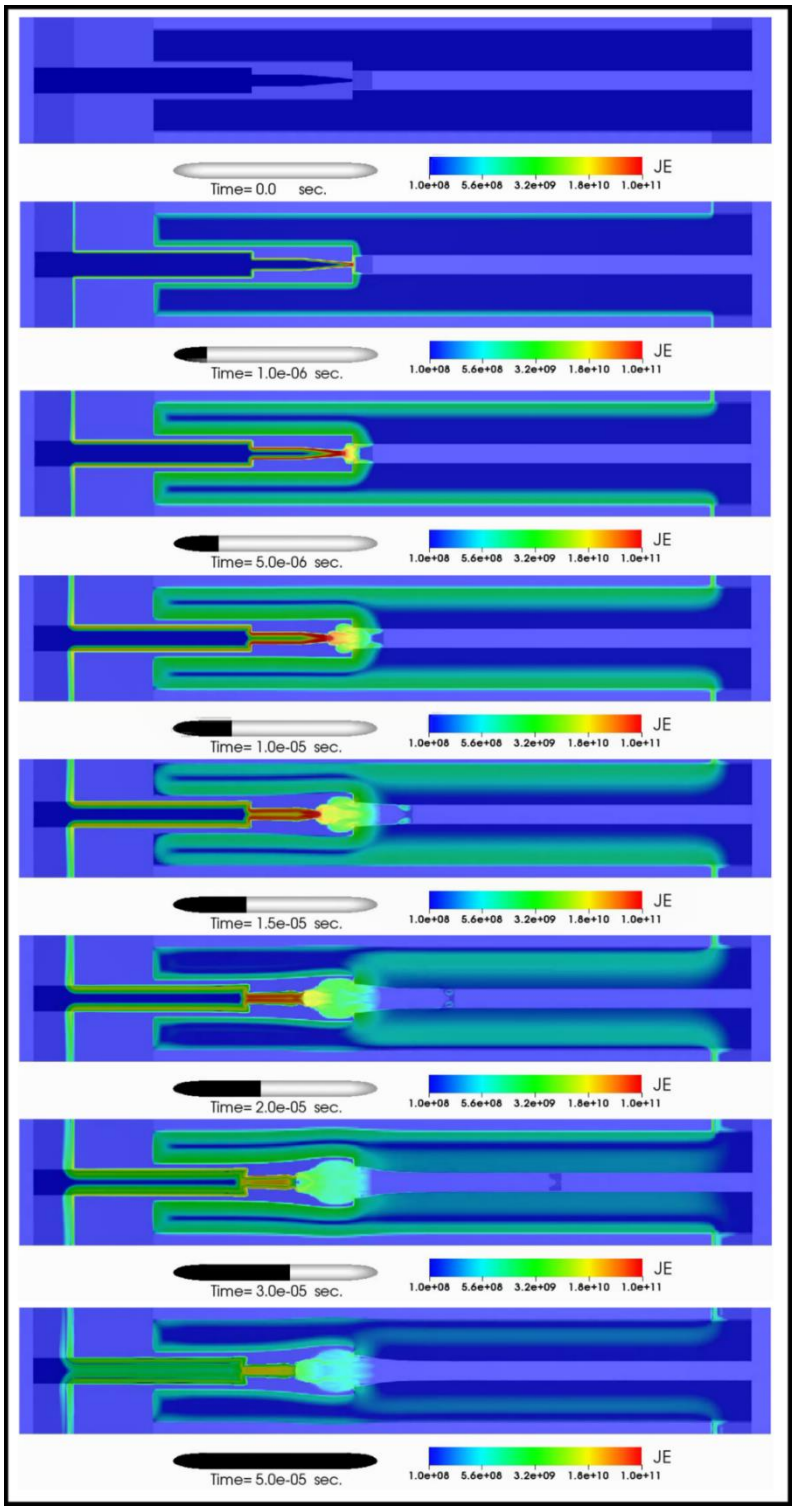

Fig. 20 Current density observed in a 3-D ALEGRA simulation of an L/D = 4 electrode tip

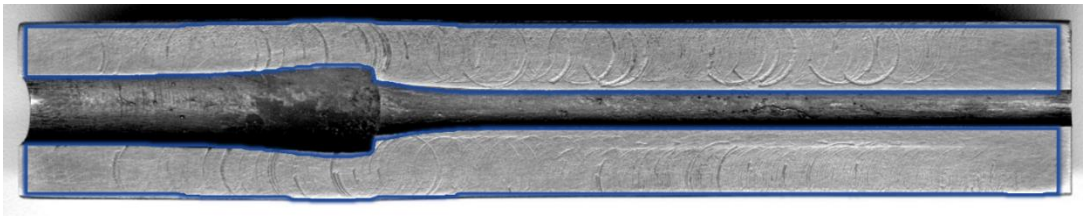

Fig. 21 Image of the sectioned barrel from shot 3 with an ALEGRA simulation of the barrel expansion outlined and overlaid in blue

The simulation captured in Fig. 20 induces a velocity in the projectile of 3020 m/s and is directly compared in Fig. 22 to the PDV data captured in shot 6, which had a peak velocity of 2978 m/s. The simulated velocity plot was produced by a Lagrangian tracer at the front center of the projectile. The correlation is better than expected both in final velocity and the acceleration profile.

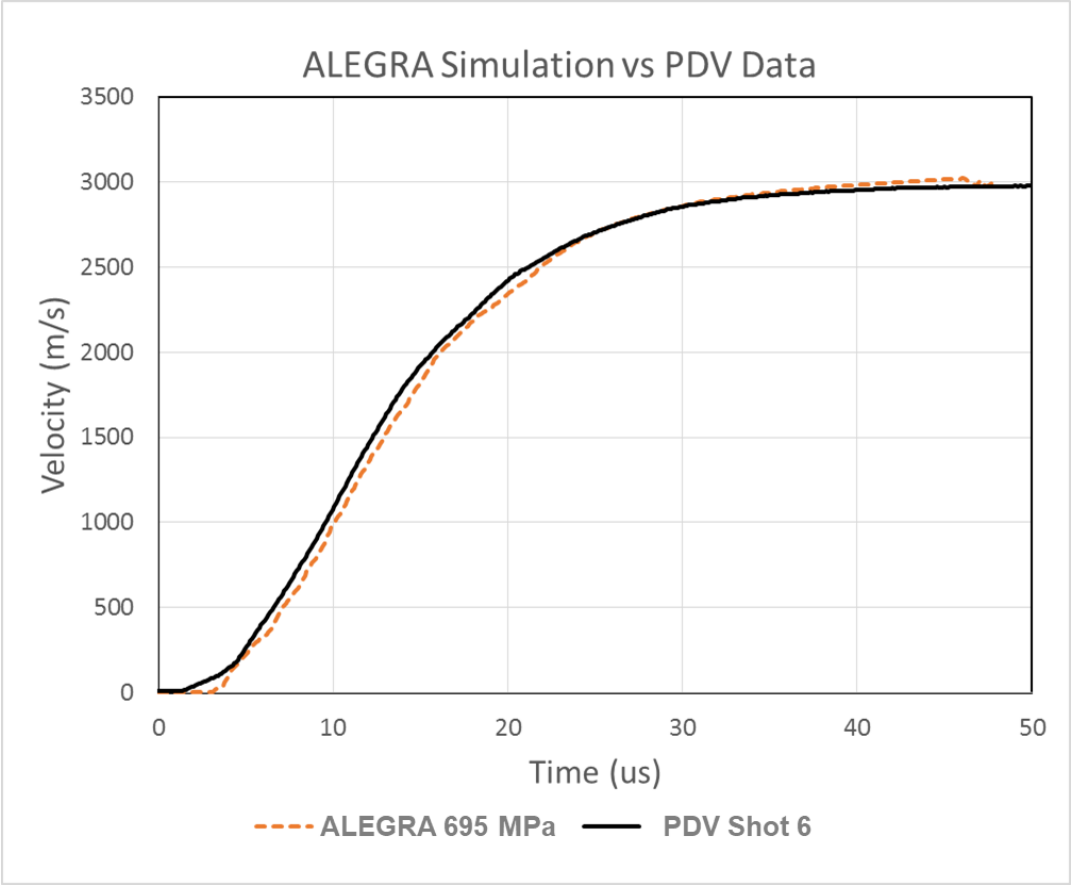

Fig. 22 Direct comparison of projectile velocity generated in an ALEGRA simulation of an electrothermal gun with L/D = 4 electrode and a barrel material yield strength of 695 MPa to the PDV data acquired in shot 6

Simulations showed that the yield strength of the barrel had a significant impact on the final velocity of the projectile. As illustrated in Fig. 23, the initial acceleration was nearly identical, then the velocity curves began to diverge after about 10 μs, at which point the projectile has only traversed about 5 mm or one length of the pellet. According to the simulations, the chamber area of the barrel has yet to begin expansion, and the only observable expansion is in the region of the barrel bore, which had been vacated by the pellet. Thus, even the small expansion observed in the bore is a significant contributor to a less efficient acceleration. After 15 μs, the chamber has begun to expand and the divergence in velocities for barrels of varying strengths/hardness is considerable (nearly 1300 m/s from 470- to 1400-MPa barrels). Final velocities range from 2460 to 3720 m/s.

As a result of these simulations, it is clear that hardening of the barrel can significantly increase performance. Thus, the barrel used in shot 9 was heat treated for hardening after machining. A final reaming of the bore to 4.76-mm precision was then performed. A measurement of the hardness on the outer section of the barrel resulted in a Brinell hardness of 387, corresponding to a yield strength of 1276 MPa, as mentioned in Section 5. The simulation closest in hardness used a yield strength of 1200 MPa. Additionally, the center may not have hardened as much as the outer portion of the barrel, thus the slightly softer simulation of 1200 MPa was used for a direct comparison. The inset of Figure 23 shows the chamber expansion difference between the 695- and 1200-MPa simulations at 30 μs.

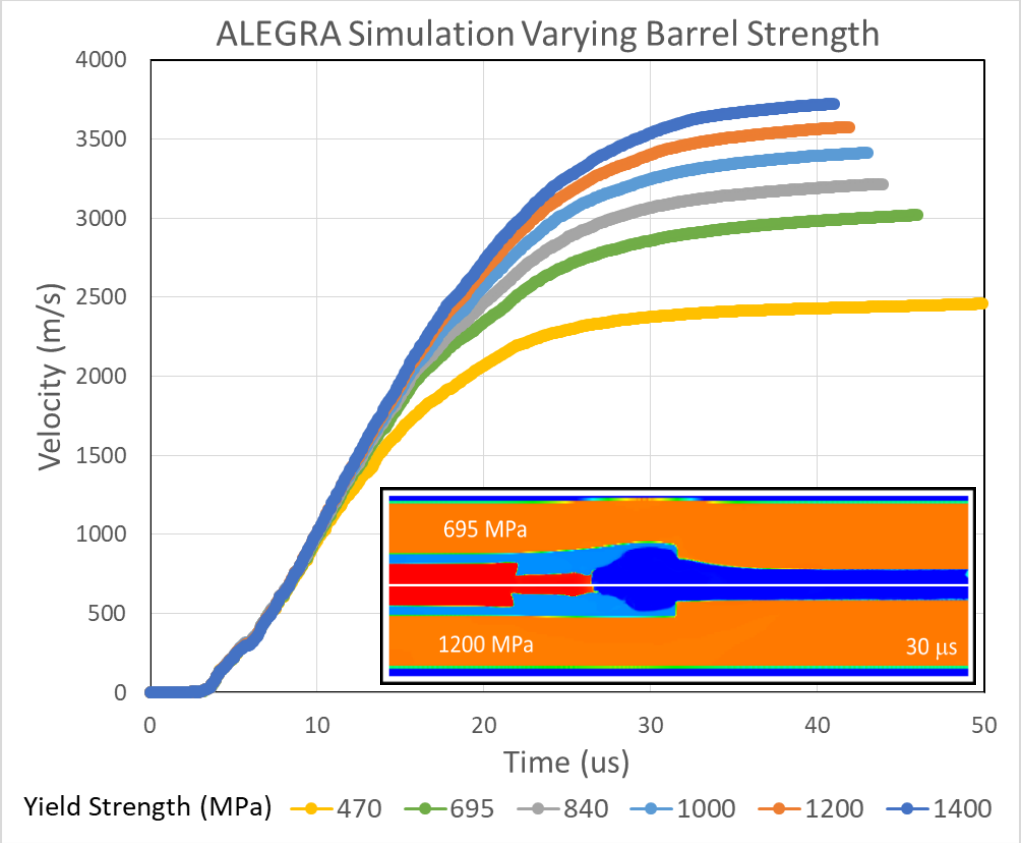

Fig. 23 Velocity profiles from ALEGRA simulations utilizing various barrel strengths. The inset shows the simulation difference in barrel expansion between the barrel steel as purchased and hardened (approximately the hardness used in shot 9).

Simulated projectiles reached a velocity of 3575 m/s before exiting the 1200 MPa barrel; 4.6% higher than shot 9 velocity of 3410 m/s. Figure 24 shows the PDV and simulation comparison. The PDV for shot 6 is again shown for contrast to the increased performance. While the simulations predicted an 18% increase in velocity, the experiment also yielded a significant increase of 15%. PDV data collected thus far show most of the experiments initially increasing in velocity at less than 1.5 µs, whereas shot 9 begins at 3 µs, which is very close to the start of acceleration in the simulations. However, the simulations and other experiments have a greater acceleration below 12 µs. The only other experiment that has a slope similar to shot 9 is the L/D = 5 electrode case of shot 12. It is unknown what bearing this had on the final velocity.

The ALEGRA simulations proved to be a very useful design tool in furthering the performance of the gun. The replication of the experimental results concerning both the chamber expansion and final velocities is very promising. Investigations analyzing the potential effects of small gaps at the electrode/pellet interface and/or air bubbles in the epoxy surrounding the electrode on the acceleration and final

velocity will be addressed in a future report. Additional work is being performed on simulating the pellet/bore interface because excessive erosion of the pellet is occurring in the simulations (see Fig. 20 at 30 μs, only half of the pellet remains). Because Eulerian simulations "weld" interfaces, excessive friction occurs along the pellet and mass is lost that is not lost in experiments. However, since the aluminum pellet is much softer than the barrel, it yields and the pellet accelerates smoothly. To produce a more correct simulation, this issue is being addressed. While acknowledging these weaknesses in the ALEGRA simulations, the simulations had a direct impact on the advancement of this work.

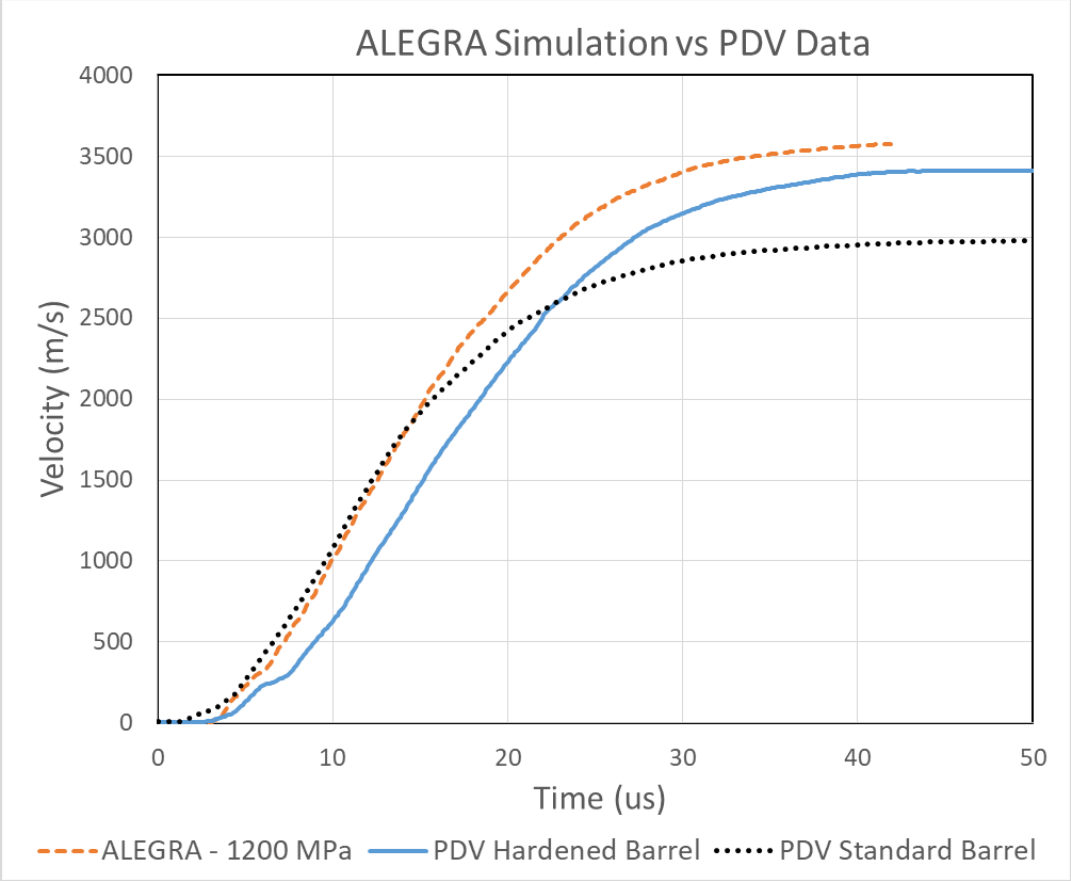

Fig. 24 Comparison of the 1200 MPa yield strength barrel ALEGRA simulation and PDV of the hardened barrel result of shot 9 and standard barrel result of shot 6

7. Conclusions

Three goals were set at the beginning of this test series. One was to increase repeatability in experimental results. The second was to improve the reliability of the capacitor bank driving the gun. The third was to develop an understanding of the important parameters in the gun design that affect performance.

The first two goals were accomplished by redesigning the capacitor bank and gun hardware. The new ICAR capacitor bank has performed well with no capacitor failures. Measurements also show that more energy is being transferred to the gun mount than with the previous system, creating a more efficient system. The new gun barrel and electrode design has improved the system repeatability. The new barrel uses a thicker wall to prevent breech rupture and has a reamed barrel to reduce friction. The electrodes have CNC machined tips instead of hand ground points to guarantee geometry uniformity in all the experiments. The results of these efforts can be seen in experiments 3, 4, and 6, which were identical experiments other than the instrumentation used to record projectile velocity. Averaging all the projectile velocity measurements from those three experiments yields a value of 2955 m/s, with a range of only ±1.2%. The complex geometry tip in experiment 10 yielded nearly the same velocity of 2950 m/s.

Previous work had indicated that the projectile velocity was sensitive to the taper angle of the electrode tip, with an L/D ratio of four identified as the optimum value. In this work, experiments 6, 8, 11, and 12 had the same nominal electrode diameter, but had L/D ratios of 4, 2, 3, and 5, respectively. The tips with an L/D ratio of 4 and 5 performed nominally the same. The L/D = 2 tip performed worst, with a velocity significantly lower. The tip taper with the best performance was L/D = 3, which yielded a slightly higher projectile velocity of 3070 m/s.

None of the experiments that used tubes as electrodes performed well. A solid tip design seems to perform better in general. This may be due to the increased mass of copper in the solid tips. As hypothesized in the prior work (see Appendix A), it is believed that vaporized copper is the working fluid in the breech creating the pressure to drive the projectile. The electrodes with tube tips may have starved the breech of working fluid mass.

Two experiments were performed with different insulating materials to determine insulator effect. Both the mica and Bakelite insulators performed worse than the standard Teflon insulator.

One experiment was performed with a larger diameter tip of 4.76 mm using the standard L/D = 4 tip taper. This geometry performed well with a higher projectile velocity of 3132 m/s.

The largest effect on projectile velocity came from heat treating the barrel to increase steel strength. Increasing the strength of the steel from 731 to 1276 MPa resulted in a 15% increase in projectile velocity to 3410 m/s. The higher strength steel resulted in less deformation to the breech, reducing the breech volume. As a result, the breech pressure was higher, increasing the propelling force on the projectile.

The simulations did a good job of matching the gun performance with the L/D = 4 geometry electrode tip. The simulations were able to match projectile muzzle velocity and the acceleration of the projectiles in the barrel with the exception of the first few microseconds. The simulations also reproduced the experimental finding that increased barrel strength improves projectile velocity. However, it overpredicts the final velocity of experiment 9 with a velocity of 3575 m/s compared to the recorded velocity of 3410 m/s. The simulated cross section of the lower strength steel barrel matches well with the sectioned barrel from the experiment.

8. References

1. Uhlig WC, Heine A. Electromagnetic diagnostic techniques for hypervelocity projectile detection, velocity measurement, and size characterization: Theoretical concept and first experimental test. Journal of Applied Physics. 2015;118:184901.

2. Strand OT, Goosman DR, Martinez C, Whitworth TL, Kuhlow WW. Compact system for high-speed velocimetry using heterodyne techniques. Review of Scientific Instruments. 2006;77(8):1–9

3. Robinson AC, Brunner TA, Carroll S, Drake R, Garasi CJ, Gardiner T, Haill T, Hanshaw H, Hensinger D, Labreche D, et al. ALEGRA: an arbitrary Lagrangian-Eulerian multimaterial, multiphysics code. Proceedings of the 46th AIAA Aerospace Sciences Meeting; 2008. Paper AIAA-2008-1235.

Appendix A. Prior Work

As described in the main body of this report, the earliest proof-of-principle experiments were done with the gun design pictured in Fig. A-1. The initial gun concept and this particular gun design were developed by Aaron Bard of the US Army Combat Capabilities Development Command's Army Research Laboratory.

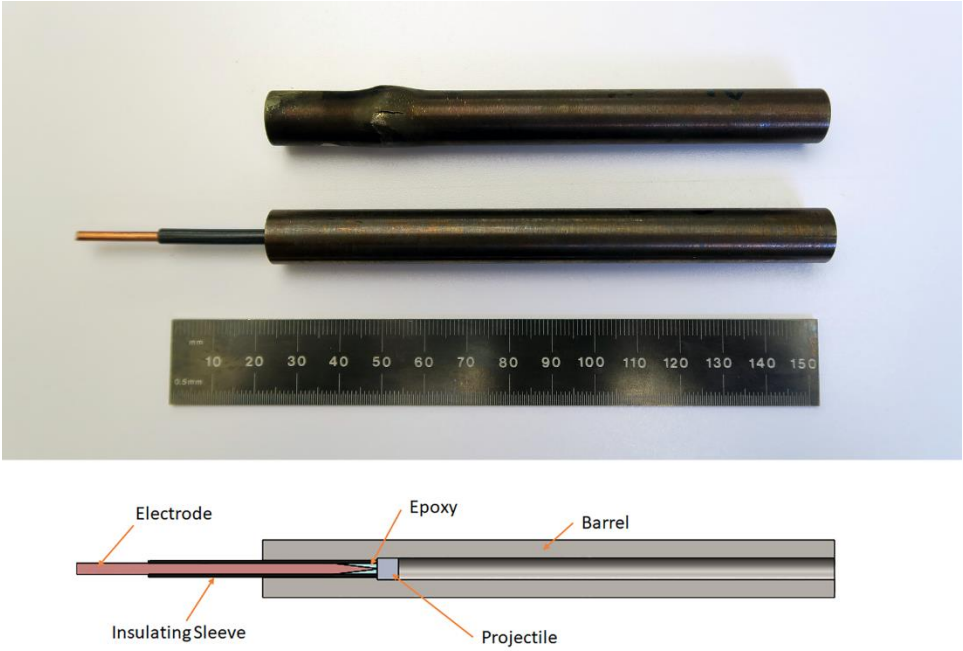

Fig. A-1 Original electrothermal gun geometry (scale is in mm)

This design utilized a barrel with an inner diameter (ID) of 4.76 mm (3/16 inch) and a breech electrode wire chamber with an ID of 3.81 mm (0.15 inch). The overall gun was 127 mm (5.0 inches) long and had an outer diameter (OD) of 12.7 mm (0.5 inch). The barrel portion was 101.6 mm (4 inches) long and the breech portion was 25.4 mm (1 inch) long.

The breech electrode or anode rod, which in most shots consisted of pure copper, was 2.38 mm (3/32 inch) in diameter and was insulated with a section of jacket stripped from 10-AWG wire. A point was hand ground on each electrode rod to ensure that the arc initiated on the center of the back of the projectile. The most common projectile used was an length/diameter (L/D) = 1 right circular aluminum cylinder. Other projectiles included L/D = 1 grade 5 titanium cylinders, precision ground aluminum spheres, and silicon carbide (SiC) spheres.

As mentioned in the main body, these guns were powered by a single Maxwell (now General Atomics) model 32511 capacitor, with a nominal capacitance of 175 µF and a typical measured capacitance of 180 µF, such that, at 20 kV, these capacitors store 36 kJ. Using an initial charge voltage of 20 kV, the peak currents achieved were on the order of 350 to 400 kA, which is 5 to 10 times higher than

most capacitors of this type are rated to supply. This greatly curtailed the lifetime of the capacitors used in these experiments and several failed completely during testing.

The time rate of change of the current (*I*-dot) was measured with a calibrated Rogowski coil and the voltage difference (*V*) across the gun mount was measured with two Northstar model PVM-2 high-voltage probes. Current as a function of time (*I*(*t*)) was determined by numerical integration of the *I*-dot signal, and the overall energy delivered to the gun mount was determined by numerically integrating the product *I***V*. Velocity was measured using high-speed video or the previously described make light system.

Figure A-2 contains a plot of a typical current pulse from one of the experiments, alongside a simulated LRC circuit pulse. As in all the experiments discussed here, the initial voltage was 20 kV. While the experimental pulse roughly resembles the LRC circuit simulation, it is clear that the resistance of the experimental circuit is not perfectly constant over time, as is assumed in the LRC circuit simulation.

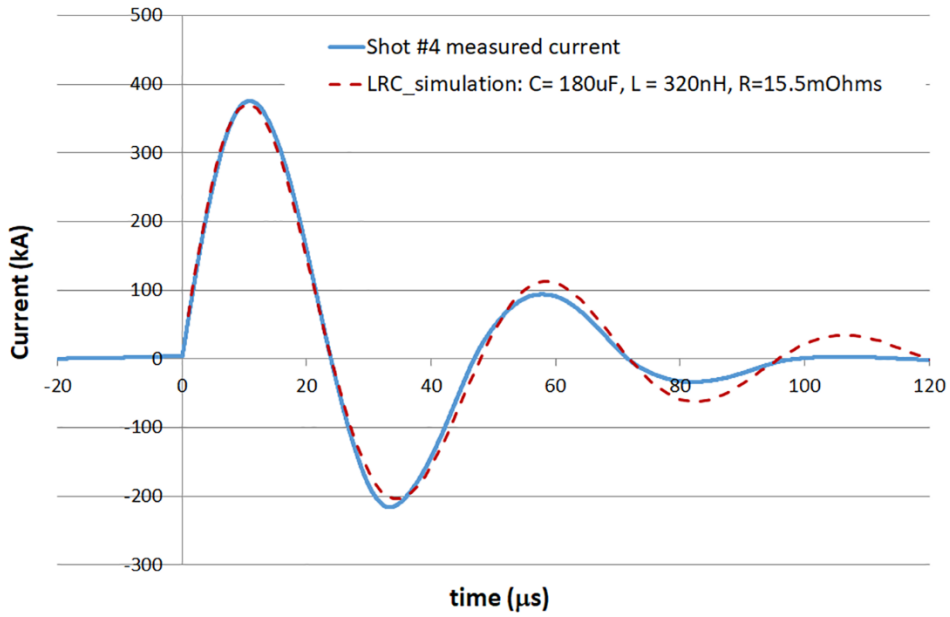

Fig. A-2 Typical current pulse

Figure A-3 contains a plot of the energy supplied to the gun mount as a function of time. The maximum energy supplied is 14.1 kJ, or about 39% of the energy stored in the capacitor at the start. This is typical of all the shots that used a copper electrode rod. This low transfer efficiency is due to the fact that much of the resistance in the circuit is parasitic in nature, contained within the capacitor itself. This is another indication that these capacitors are not an appropriate source for 375-kA pulses.

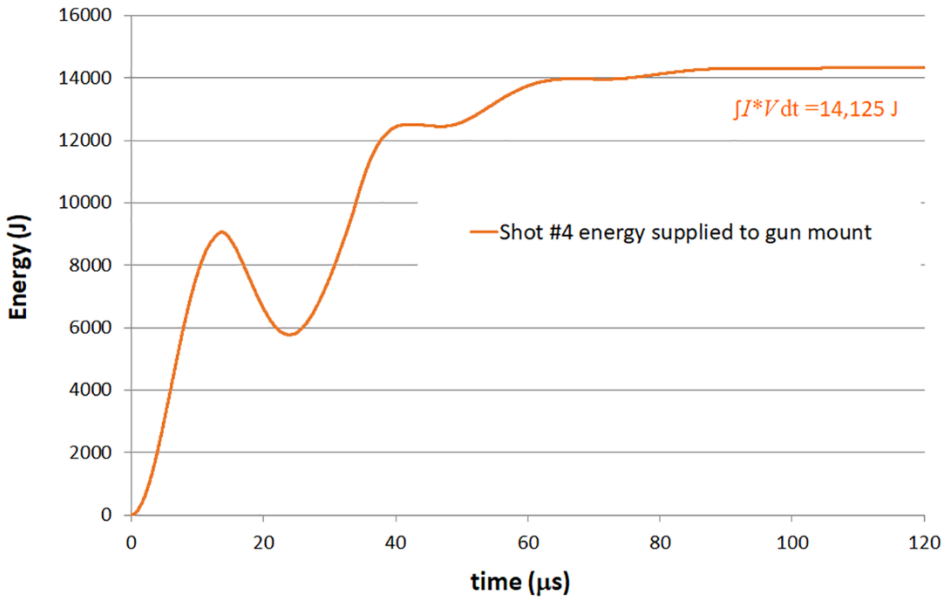

Fig. A-3 Energy supplied to the gun mount

The main goal of this early work was to see how performance changed when various aspects of the design were varied. Rather than describe every shot, a simple summary of results is presented. Aspects that were varied include projectile type, breech electrode rod (anode) composition, barrel length, and the breech electrode point L/D ratio. Figure A-4 shows a plot of all projectile velocities measured as a function of the mass of the projectiles fired. The line is a guide for the eye. As can be seen, there is a definite dependence on projectile mass as well as a large variation from shot to shot for any given projectile type.

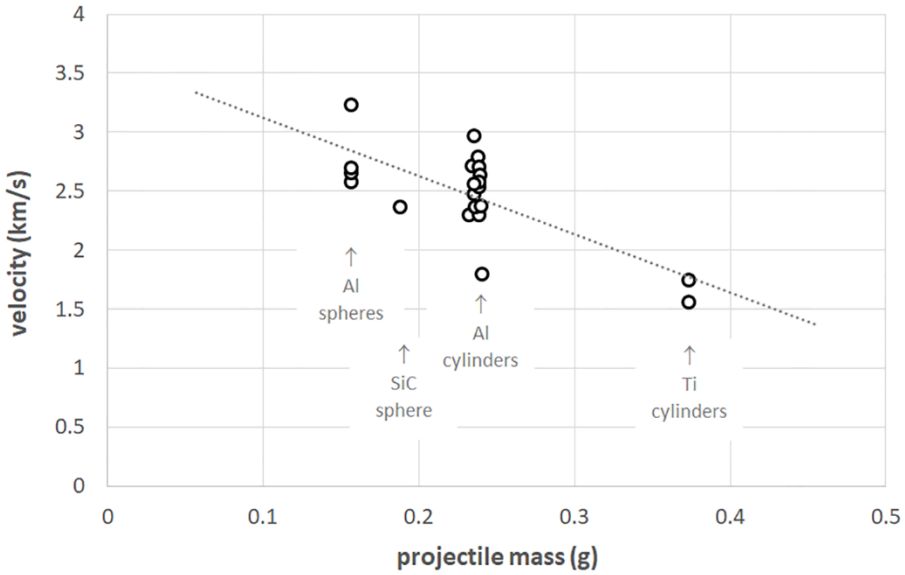

Fig. A-4 Projectile velocities as a function of projectile mass

Note that while the aluminum spheres had significantly less mass than the aluminum cylinders, the average sphere velocity was only slightly larger than the average cylinder velocity. This discrepancy is magnified when one compares the kinetic energies of the projectiles as is done in Fig. A-5, where it is evident that the average kinetic energy of the aluminum cylinders is in fact higher than the average kinetic energy of the aluminum spheres (the line is a guide for the eye). This effect was attributed to increased blow-by of the propelling gasses in the sphere cases, making the cylinders the more efficient choice overall.

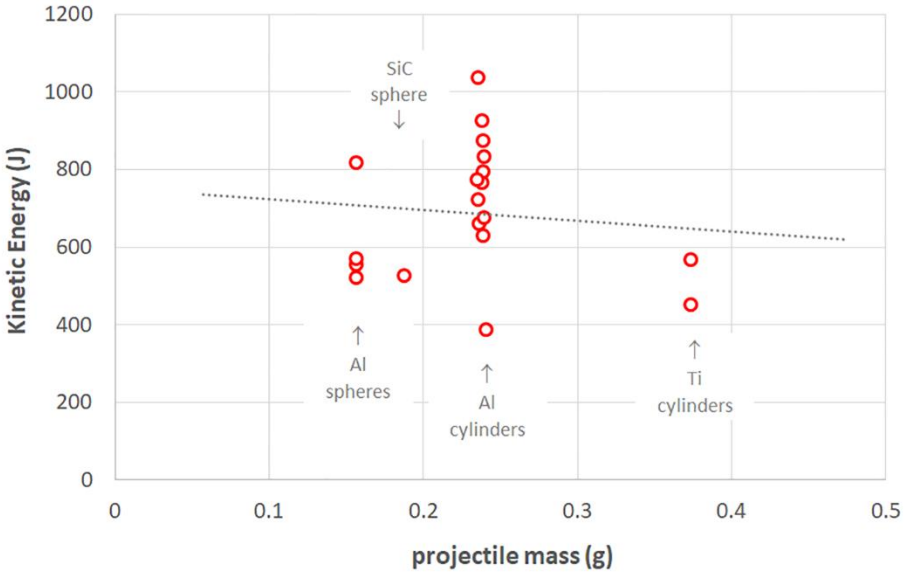

Fig. A-5 Projectile kinetic energy as a function of projectile mass

While some of the variation seen in the velocities measured was due to intentional design variations (e.g., the use of both aluminum and tungsten breech electrode rods resulted in subpar velocities), the variation seen in designs that should have performed the same was still quite large. In the case of cylindrical aluminum projectiles, values ranged from 2.3 to 2.9 km/s. The cause of this was eventually determined to be variations in the shape of the hand-ground point on the copper anode. This was verified by carefully grinding the points with varying L/D ratios and measuring the resulting velocities, using cylindrical projectiles. The results of that study are listed in Table A-1. Figure A-6 contains a photograph of an anode with an L/D = 2.7 point.

Table A-1 Results of the anode point shape study

Shot #	Anode L/D	Pellet velocity (km/s)
18	4	2.63
19	4	2.57
20	4	2.56
21	5.3	1.79
22	1.1	2.36
23	2.7	2.37

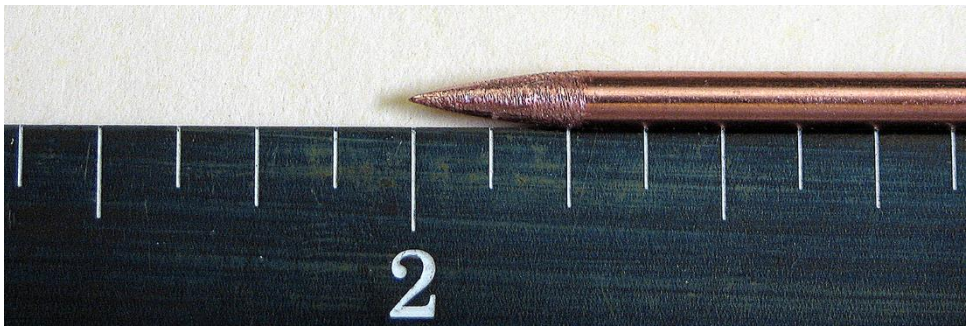

Fig. A-6 A hand-ground L/D = 2.7 anode point (scale is in inches, 1 inch = 25.4 mm)

The results of the L/D study not only explained the random variation in the velocities measured, they also shed light on another mystery: the nature of the working fluid. The sensitivity to L/D ratio was taken to mean that vaporized copper was the main component in the working fluid, and that the shape of the point on the copper anode determined the rate at which the vapor could be supplied during the acceleration process. It is clear from the study that an L/D of around 4 was the optimal shape for producing copper vapor in a timely fashion, at least in this gun design.

Appendix B. Experimental Data Recorded

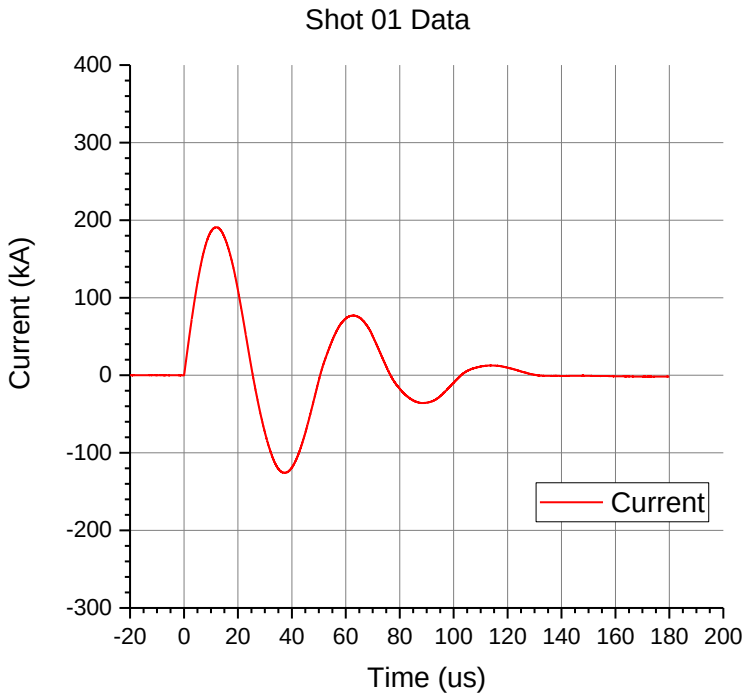
Shot 01 Data
Current (kA)
400
300
200
100
0
-100
-200
-300
-20
0
20
40
60
80
100
120
140
160
180
200
Time (us)
Current

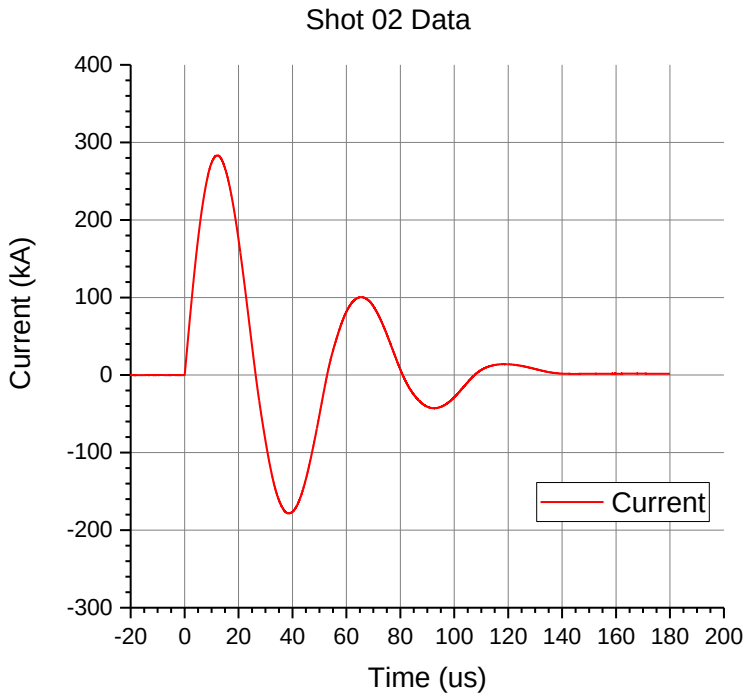
Shot 02 Data
Current (kA)
400
300
200
100
0
-100
-200
-300
-20
0
20
40
60
80
100
120
140
160
180
200
Time (us)
Current

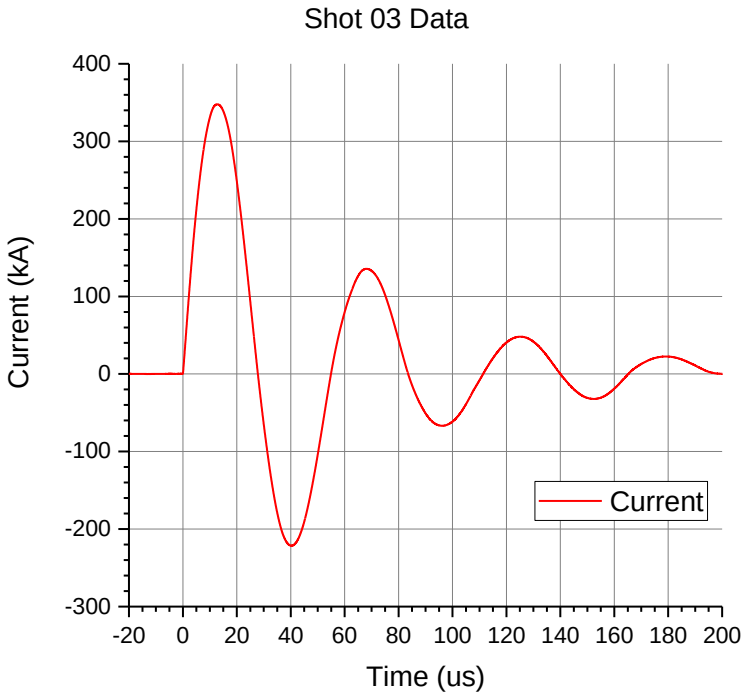
Shot 03 Data
Current (kA)
400
300
200
100
0
-100
-200
-300
-20
0
20
40
60
80
100
120
140
160
180
200
Time (us)
Current

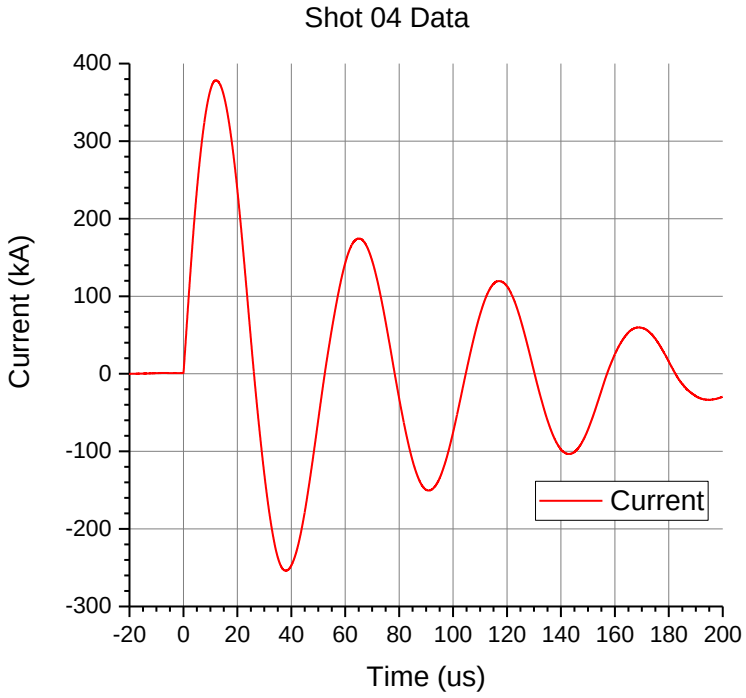
Shot 04 Data
Current (kA)
400
300
200
100
0
-100
-200
-300
-20
0
20
40
60
80
100
120
140
160
180
200
Time (us)
Current

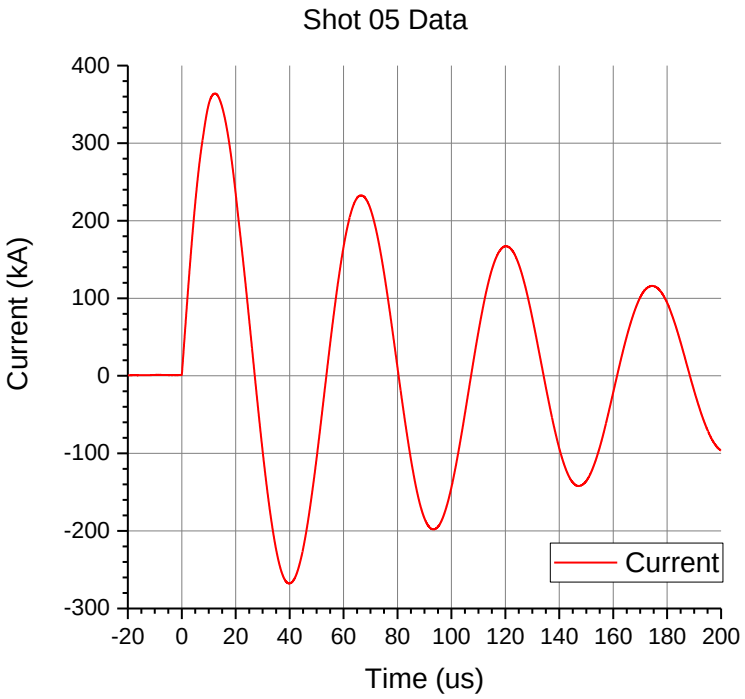
Shot 05 Data
Current (kA)
Time (us)
Current
400
300
200
100
0
-100
-200
-300
-20
0
20
40
60
80
100
120
140
160
180
200

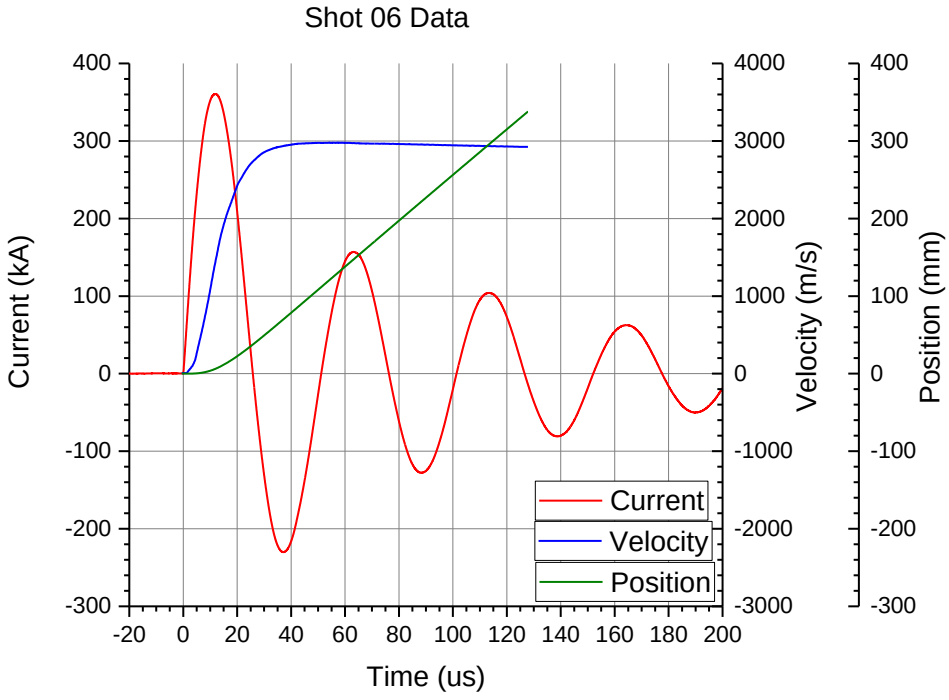
Shot 06 Data
Current (kA)
Velocity (m/s)
Position (mm)
Time (us)
Current
Velocity
Position
400
300
200
100
0
-100
-200
-300
4000
3000
2000
1000
0
-1000
-2000
-3000
-20
0
20
40
60
80
100
120
140
160
180
200

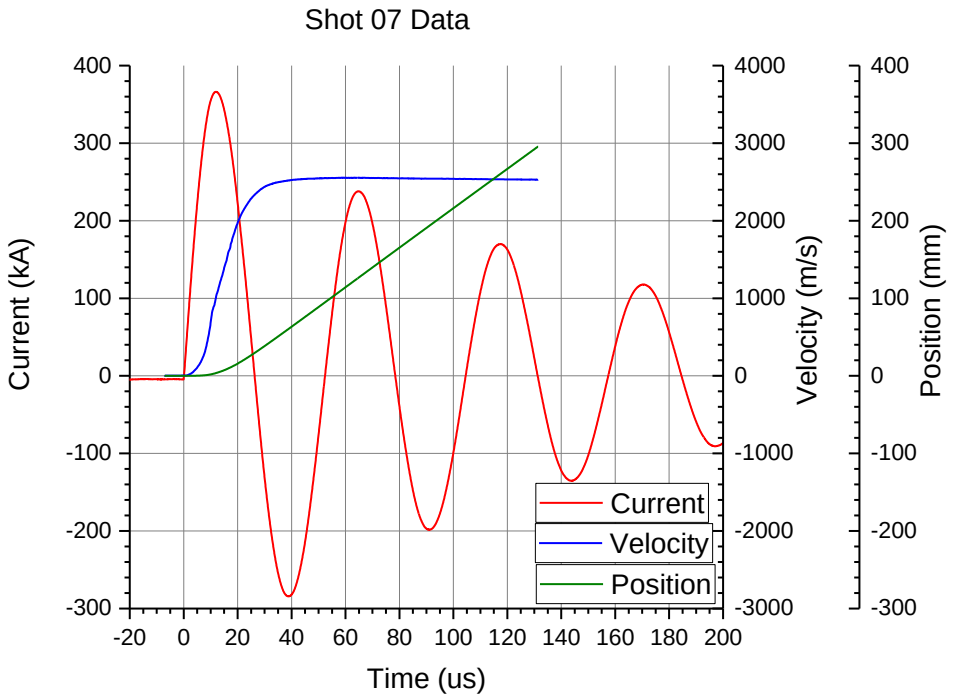
Shot 07 Data
Current (kA)
Velocity (m/s)
Position (mm)
Time (us)
Current
Velocity
Position

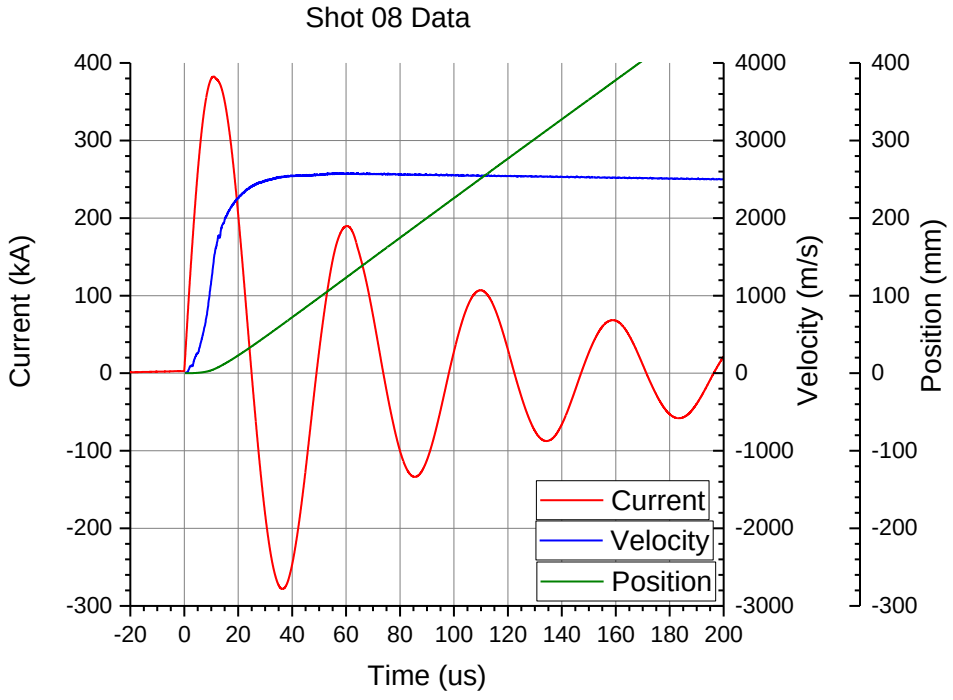
Shot 08 Data
Current (kA)
Velocity (m/s)
Position (mm)
Time (us)
Current
Velocity
Position

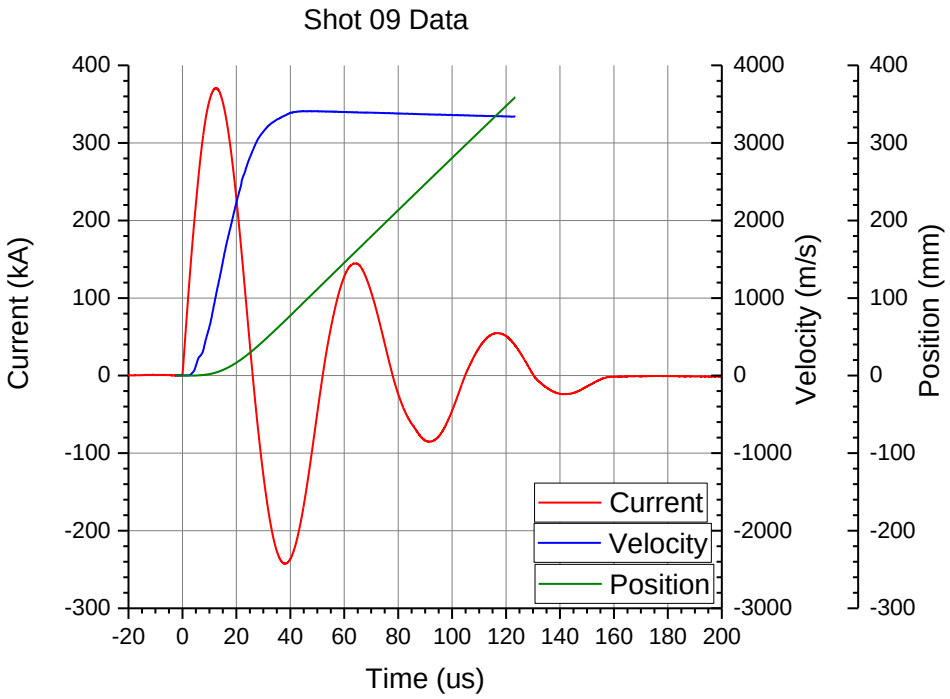
Shot 09 Data
Current (kA)
Velocity (m/s)
Position (mm)
Time (us)
Current
Velocity
Position

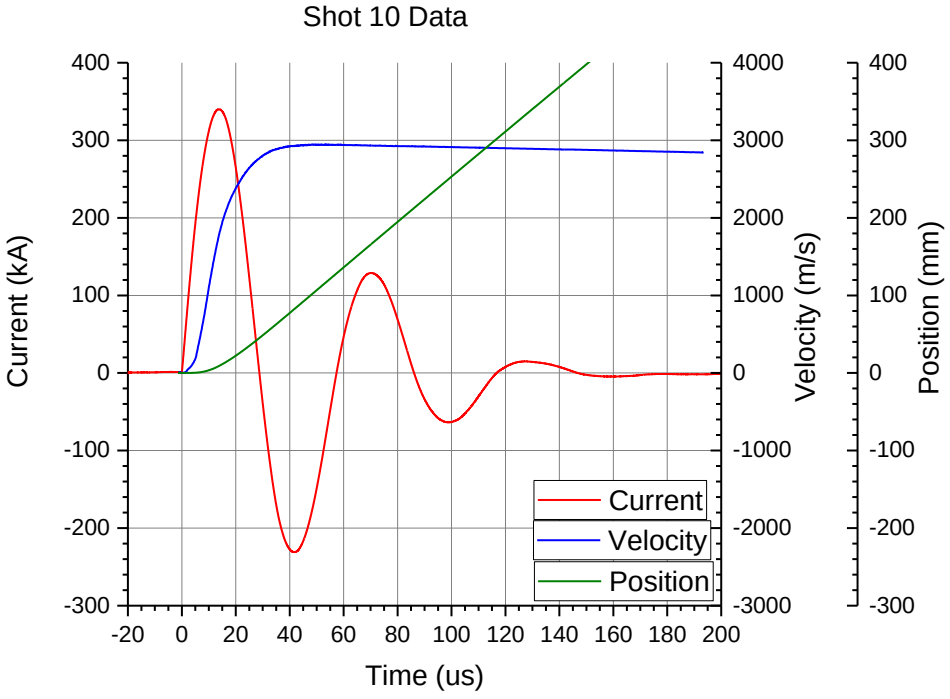
Shot 10 Data
Current (kA)
Velocity (m/s)
Position (mm)
Time (us)
Current
Velocity
Position

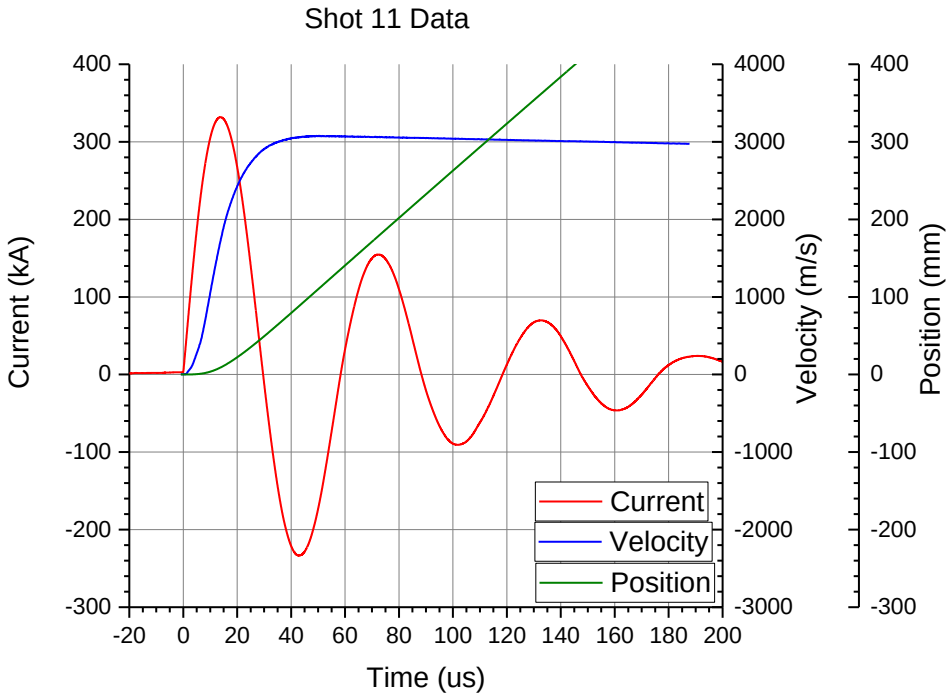
Shot 11 Data
Current (kA)
Velocity (m/s)
Position (mm)
Time (us)
Current
Velocity
Position

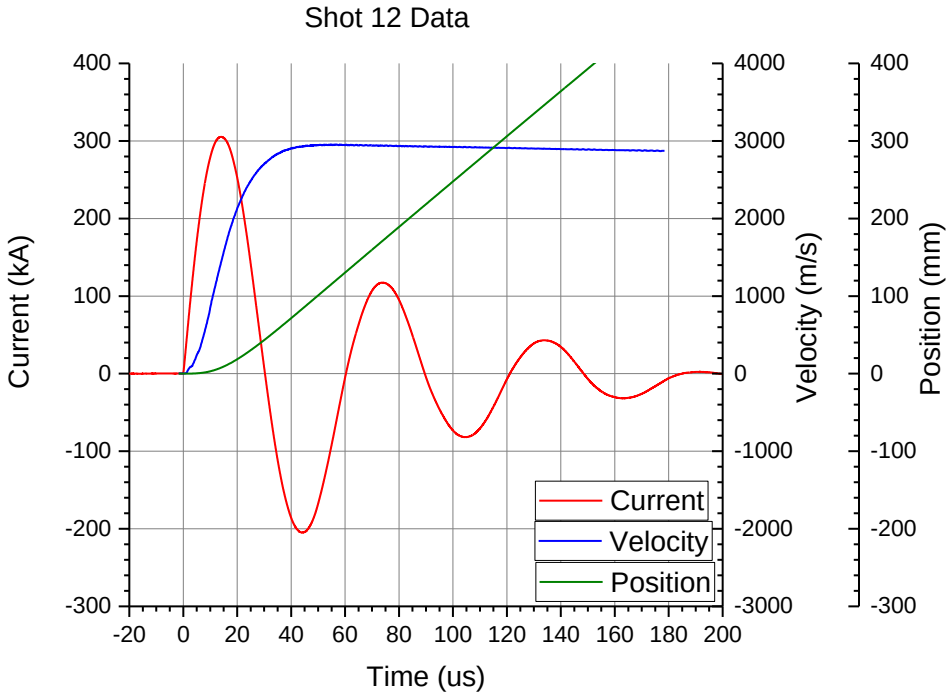
Shot 12 Data
Current (kA)
Velocity (m/s)
Position (mm)
Time (us)
Current
Velocity
Position

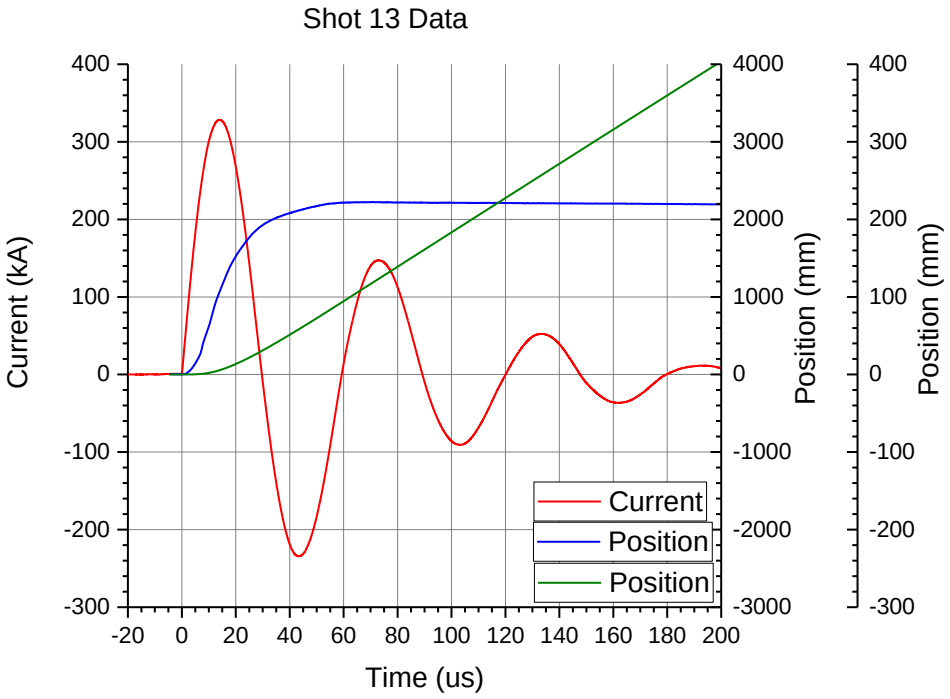
Shot 13 Data
Current (kA)
Position (mm)
Position (mm)
Time (us)
Current
Position
Position

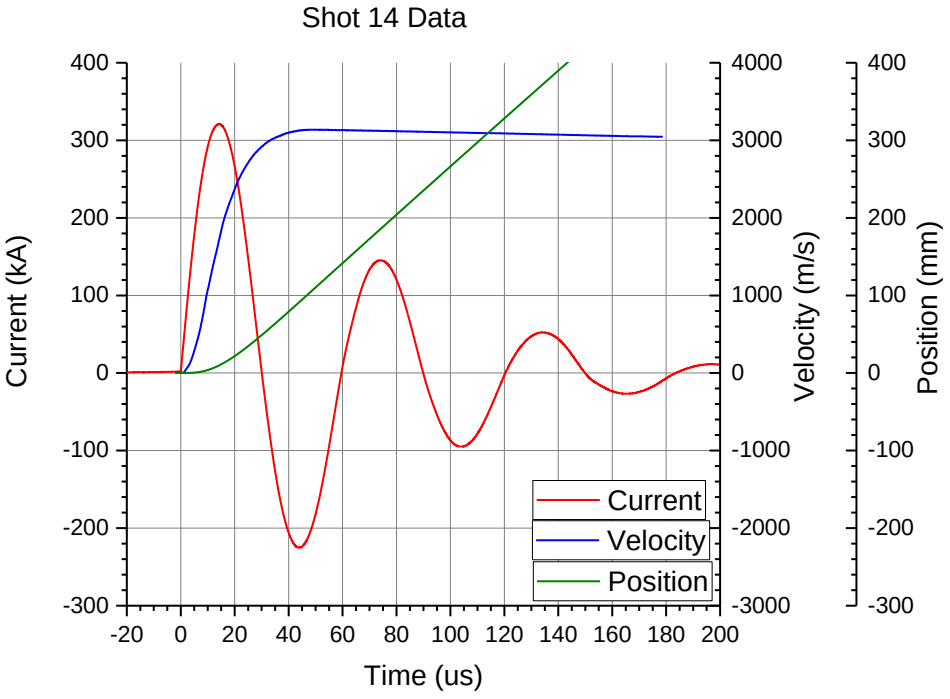
Shot 14 Data
Current (kA)
Velocity (m/s)
Position (mm)
Time (us)
Current
Velocity
Position

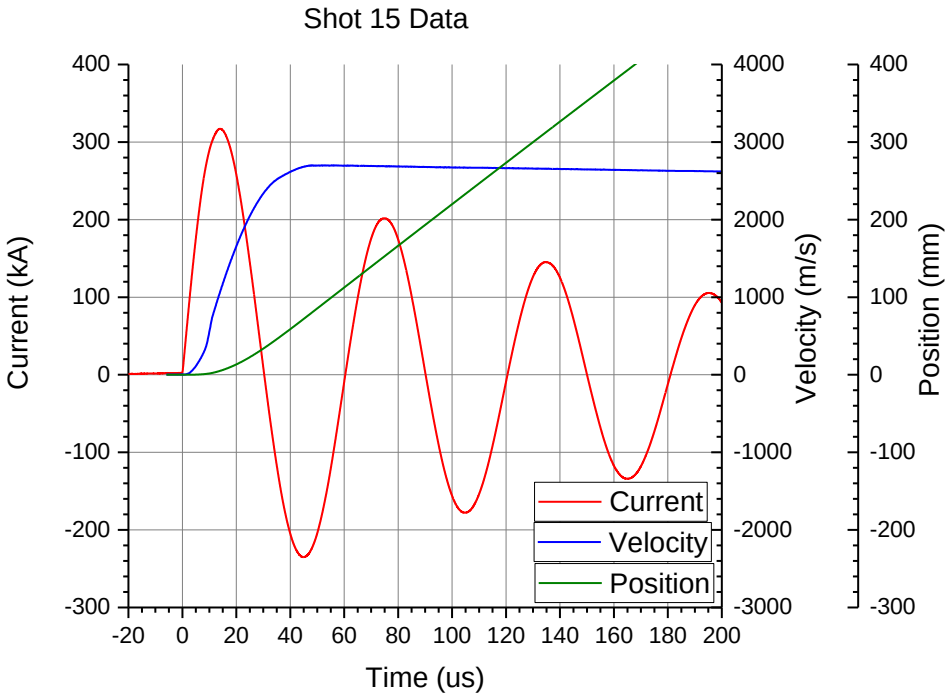
Shot 15 Data
Current (kA)
Velocity (m/s)
Position (mm)
Time (us)
Current
Velocity
Position

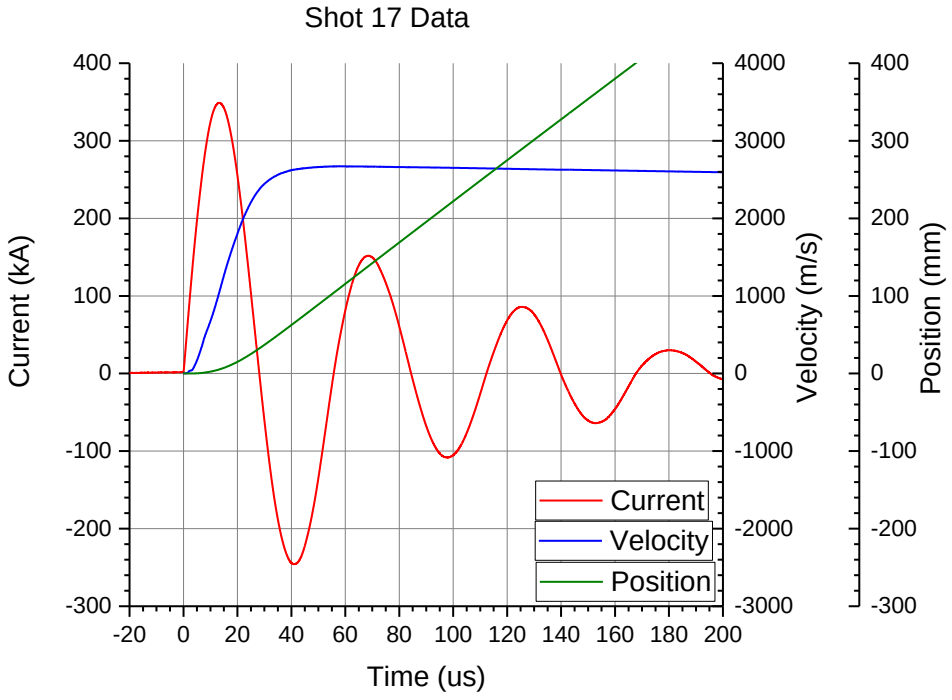
Shot 17 Data
Current (kA)
Velocity (m/s)
Position (mm)
Time (us)
Current
Velocity
Position

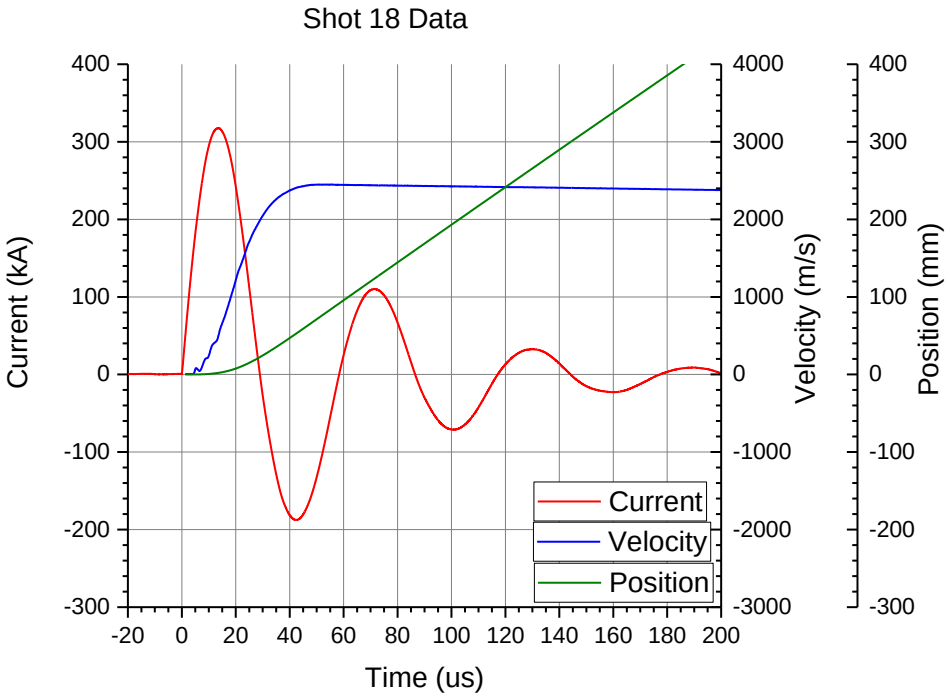
Shot 18 Data
Current (kA)
Velocity (m/s)
Position (mm)
Time (us)
Current
Velocity
Position
400
300
200
100
0
-100
-200
-300
4000
3000
2000
1000
0
-1000
-2000
-3000
-20
0
20
40
60
80
100
120
140
160
180
200

List of Symbols, Abbreviations, and Acronyms

ARL	Army Research Laboratory
CCDC	US Army Combat Capabilities Development Command
CNC	computer numerical control
di/dt	current derivative
HS	high speed
ID	inner diameter
L/D	length/diameter
OD	outer diameter
PDV	Photon Doppler Velocimetry
PTFE	polytetrafluoroethylene
PVC	polyvinyl chloride
SiC	silicon carbide

1 (PDF) DEFENSE TECHNICAL INFORMATION CTR DTIC OCA

2 (PDF) DIR ARL IMAL HRA RECORDS MGMT FCDD RLD CL TECH LIB

1 (PDF) GOVT PRINTG OFC A MALHOTRA

37 (PDF) ARL FCDD RWL D LYON S SCHOENFELD FCDD RWL PA S BILYK J FLENIKEN M MCNEIR C WOLFE P BERNING M COPPINGER W UHLIG L VANDERHOEF J CAZAMIAS B WILMER FCDD RLW PC S SEGLETES R BECKER D CASEM FCDD RLW PD J RUNYEON M KEELE F MURPHY C RANDOW D KLEPONIS A BARD N BRUCHEY S SCHRAML R MUDD R DONEY G VUNNI M ZELLNER FCDD RLW PE P SWOBODA P BARTKOWSKI D GALLARDY D HACKBARTH D HORNBAKER K KRAUTHAUSER FCDD RLW PF N GNIAZDOWSKI FCDD RLW PB C HOPPEL FCDD RLS DP C TIPTON D PORSCHET

6 (PDF) US ARMY TACOM J WHITE L FRANKS D TEMPLETON M LAWSON J HITCHCOCK N COOPER

3 (PDF) PM ABCT J ROWE E BARSHAW R NICOL

4 (PDF) NATL GROUND INTLLGNC CTR D EPPERLY T SHAVER T WATERBURY D DOBROWOLSKI

1 (PDF) PM MRAP J PEREZ (JPO)

1 (PDF) DARPA/DSO L CHRISTODOULOU

1 (PDF) PM BFVS D SPENCER

1 (PDF) NSWC CARDEROCK DIV R PETERSON

1 (PDF) SANDIA NATL LAB E STRACK

2 (PDF) LAWRENCE LIVERMORE NATL LAB A JOHNSON J SOLBERG

1 (PDF) LOS ALAMOS NATL LAB D REISMAN

2 (PDF) BAE SYSTEMS LANDS & ARMAMENTS R APPLETON

1 (PDF) GDLS M KAUTZER

1 (PDF) US ATEC E SANDERSON